This is the Author Submitted version (preprint) of the following paper:

The Potential of ALOS-2 and Sentinel-1 Radar Data for Soil Moisture Retrieval with High Spatial Resolution over Agro-forestry Areas, China

Huizhen Cui, Lingmei Jiang, *Member, IEEE*, Simonetta Paloscia, *Fellow, IEEE*, Emanuele Santi, *Member, IEEE*, Simone Pettinato, Member, IEEE, Jian Wang, Xiyao Fang, Wanjin Liao

Abstract—Synthetic aperture radar (SAR) sensors, such as Advanced Land Observing Satellite-2 (ALOS-2) and Sentinel-1, provide significant opportunities for soil moisture content (SMC) retrieval with relatively high spatial resolutions (10~30 m). In this work, an artificial neural network (ANN) SMC retrieval algorithm combined with water cloud model, advanced integral equation model and Oh model database were proposed. The SAR co-polarization backscatter, the local incidence angle, and the normalized difference vegetation index were used in input vectors for the ANN algorithm for the retrieval and mapping of the ALOS-2 and Sentinel-1 SMC at a 30 m resolution. The results of the comparison between the SMC retrievals and the measured SMC show that Sentinel-1 and ALOS-2 SMC retrievals with high accuracy correspond to low vegetation areas (crop, grass and shrub), with a root mean square error (RMSE) of 0.021 and 0.033 cm3/cm3, respectively. ALOS-2 SMC retrievals provide higher accuracy (RMSE=0.076 cm^3/cm^3) than Sentinel-1 SMC retrievals at high vegetation (e.g., forest). However, it remains challenging for soil moisture retrieval in forest land. The C-band and L-band SMC retrievals have higher RMSE (up to 0.047cm^3/cm^3) at low incidence angle (<20 °) and high incidence angle (>50 °). In addition, by considering the impact of rainfall on the SMC, it appears that the Sentinel-1 and ALOS-2 SMC have a good response to the rainfall events. Finally, the results of the comparison between the SMC retrievals and the Soil Moisture Active Passive (SMAP) L2 SMC product show that the correlation coefficients between Sentinel-1, ALOS-2 and SMAP are higher in September when the vegetation is drying than in July when the vegetation is growing.

Index Terms—Agro-forestry area, Advanced Land Observing Satellite-2 (ALOS-2), Artificial Neural Network (ANN), Sentinel-1, soil moisture content (SMC).

I. INTRODUCTION

SOIL moisture content (SMC) is one of the most active parameters in the process of energy and water interchange between the land surface and atmosphere, and it is also a key variable for several applications in hydrological processes, bioecological processes, and biogeochemical processes [1]. High spatial resolution measurements of SMC have widespread applications in agricultural irrigation, hydrological modeling and meteorological climate forecasting [2]. Remote sensing techniques, with the launch of new sensors with improved performances in terms of accuracy and spatial resolution, provide a flexible alternative to capturing the SMC at regional and global scales, in particular using optical/thermal infrared and microwave sensors [3, 4]. Optical/thermal infrared sensors are affected by weather conditions (e.g., cloud, and rainfall), which makes them encounter difficulties in estimating the SMC continuously over space and time. Passive microwave satellites can provide a long-term series of SMC datasets for large areas. However, the satellites, which include FengYun-3B/C/D (FY-3B/C/D), Advanced Microwave Scanning Radiometer-2 (AMSR2), Soil Moisture and Ocean Salinity (SMOS), and Soil Moisture Active Passive (SMAP), have a coarse spatial resolution (25 ~36 km), which is limiting for many applications that require high spatial resolution. Active microwave remote sensing instruments, such as synthetic aperture radar (SAR) sensors, can provide observations at higher spatial resolutions and show rather high sensitivity to vegetation biomass and SMC, especially at low microwave frequencies (i.e., the C and L bands) [1, 5].

Microwave sensors that operate from the P to L band are more sensitive to variations in the SMC of bare and vegetated

Huizhen Cui, Lingmei Jiang, Jian Wang, and Xiyao Fang are with the Faculty of Geographical Science, State Key Laboratory of Remote Sensing Science, Jointly Sponsored by Beijing Normal University and the Aerospace Information Research Institute of Chinese Academy of Sciences, Faculty of Geographical Science, Beijing Normal University, Beijing 100875, China. (e-mail: cuihz@mail.bnu.edu.cn; jiang@bnu.edu.cn; wjian@mail.bnu.edu.cn; fang_xiyao@163.com)

Simonetta Paloscia, Emanuele Santi and Simone Pettinato are with the Institute of Applied Physics, National Research Council (IFAC-CNR), Florence, 1050019, Italy. (e-mail: s.paloscia@ifac.cnr.it; E.Santi@ifac.cnr.it; s.pettinato@ifac.cnr.it).

Wanjin Liao is with the State Key Laboratory of Earth Surface Processes and Resource Ecology, Ministry of Education Key Laboratory for Biodiversity Science and Ecological Engineering, College of Life Sciences, Beijing Normal University, Beijing 100875, China (e-mail: liaowj@bnu.edu.cn).

soils, which provides information for consistent soil layers [6-8]. However, most radar systems operate mainly at the C band (e.g., RADARSAT and ENVISAT) and X band (e.g., COSMO-SkyMed and TerraSAR-X). Although some preliminary studies have indicated some sensitivity of X-band signals to the SMC [9], this frequency does not represent the optimal option for SMC retrieval. The current satellite missions of Sentinel-1 with C-band SAR and Advanced Land Observing Satellite-2 (ALOS-2) with L-band SAR provide more opportunities for SMC retrieval at a high spatial resolution. At present, there are many studies that focus on SMC retrieval using Sentinel-1 data [10-14], but there is limited research on SMC retrieval using ALOS-2 [15, 16], which is mainly due to the scarce worldwide coverage and lack of image availability. Thus, the performance of ALOS-2 SAR to retrieve SMC requires further validation. At the same time, to obtain the highest accuracy and spatial resolution of the SMC product in the future, the potential of Sentinel-1 (C-band SAR) and ALOS-2 (L-band SAR) to retrieve SMC under different land surface conditions should be compared and investigated with a more in-depth approach.

In the process of SMC retrieval, both the surface roughness and vegetation cover have a significant effect on the radar signal, and therefore, they are the key issues to be considered. Some backscattering models have been developed to describe the scattering mechanisms of bare soil and vegetation surfaces. For bare soil, the most commonly adopted models are the integral equation model (IEM) [17], advanced IEM (AIEM) [18], and Oh model [19]. These models allow for simulation of the radar signals, SMC and soil roughness under specific soil conditions. Most studies use mainly vegetation models combined with bare soil models to simulate the backscattering in the vegetation-covered areas. The most popular models are the water cloud model (WCM) [20] and Michigan Microwave Canopy Scattering model (MIMICS) [21]. The input parameters of the MIMICS model are complex and sometimes difficult to obtain, which limits the widespread application of this model. WCM requires a few input parameters, and it is also simpler in implementation; as a result, it is more widely used in SMC retrieval [15, 22, 23].

Based on SAR images and these models, many SMC retrieval algorithms have been widely implemented for different land surfaces in the past [9, 15, 16, 24], which mainly include change detection approaches [10, 14, 25, 26], physical models [1, 5, 27, 28] and statistical methods [11, 30-32]. However, these retrieval algorithms are mainly applied to bare soil, sparsely vegetated surfaces, cropland and grassland, whereas limited studies have been conducted for dense vegetation areas, especially in agro-forestry areas. Agro-forestry areas are the typical pattern of shelterbelts and cropland in China's Three-North Shelter Forest Program [32]. A high spatial resolution SMC estimation is important for estimating carbon emissions and carbon storage and identifying the influence of water circulation in agro-forestry areas [3].

Over the last two decades, among the statistical approaches for retrieving SMC, artificial neural networks (ANNs) [23, 24, 33, 34] have been widely used, since they have the power to retrieve the complex, dynamic and non-linear patterns from the data, and therefore, they are widely applied in many land surface parameter retrieval studies that use remote sensing data [35-37]. In SMC retrieval, the ANN algorithm gives a better compromise in terms of the accuracy, computational time and criticality, compared with statistical algorithms based on Bayes' theorem, iteration algorithms based on the Nelder–Mead minimization method, and linear regression algorithms [24]. Subsequently, the potential of machine learning methods for SMC retrieval was investigated [22-24, 37], and the effectiveness of these methods in solving SMC retrieval problems has been proved, mainly using C-band or X-band SAR images of bare soil, grassland and cropland.

Therefore, due to the complexity of the land surface in the agro-forestry area and considering the ease of implementation of ANNs in retrieving SMC, this paper describes an algorithm based on ANNs to retrieve SMC from C-band and L-band SAR. Since it is well-known that one of the critical points of ANNs is the training phase, in this algorithm, we used a training set derived from model backscattering coefficient simulations obtained from the WCM, AIEM and Oh models that account for different land surface types and radar characteristics.

This work aims at investigating the potential of Sentinel-1 and ALOS-2 SAR data for the estimation of SMC and developing an SMC retrieval algorithm at high spatial resolution over agro-forestry areas. Currently, the SMC validation is mainly based on measured ground data [10, 22, 23, 38]. However, the spatial representation of the measured sites is limited. To better validate the retrieval results, in addition to the ground measured data, the remote sensing product SMAP L2 radiometer/radar SMC are used to intercompare the Sentinel-1 and ALOS-2 SMC estimates. The proposed approach for the retrieval of SMC in agro-forestry areas is based on an ANN algorithm trained by using WCM combined with AIEM and Oh model simulations. First, we generated a simulated database based on the calibrated WCM combined with AIEM and the Oh model. Half of the total data of the simulated parameters was used for training the ANN, and the other half of the simulated data was used for the validation of the algorithm. Second, Sentinel-1 and ALOS-2 SAR backscattering coefficient, local incidence angle, and normalized difference vegetation index (NDVI, derived from Sentinel-2 and Landsat 8) are input to the ANN to retrieve the SMC. Finally, Sentinel-1 and ALOS-2 SMC retrievals were validated based on the ground measurements and compared with SMAP L2 SMC product. This paper is organized as follows: section II presents the study area and database. Section III describes the data analysis and proposed methodology. Section IV presents and discusses the result of algorithm validation and SMC maps. Finally, the conclusions are summarized in section V.

II. STUDY AREA AND DATASET

The study was conducted in the Genhe watershed of China, which is mainly an area of agricultural and forestry ecotones. In the following, only a brief description of this study area is given because it is described in detail in other papers [3, 39]. The data used in this paper are mainly composed of in situ observations

of SMC, soil temperature, surface roughness and soil texture, Sentinel-1 and ALOS-2 SAR data, GlobeLand30 land cover information and NDVI. Considering the Genhe watershed with frequent cloud weather and the quality of the optical data, two optical satellites, namely, Sentinel-2 and Landsat 8, are selected to derive the NDVI and complement each other under cloudless conditions. To maintain the consistency of the spatial resolution, the Sentinel-1, ALOS-2, and Sentinel-2 observations in this paper were all sampled at 30m (by taking the average value of 10 m pixels, inside each 30 m pixel).

A. In situ data

The Genhe watershed is the northernmost and coldest area in Inner Mongolia, and it is mainly a zone of interspersed agriculture, grassland and forestry. As shown in Fig. 1, the SMC and soil temperature observation network was deployed on both sides of the Genhe watershed (50.16 °-50.66 °N, 120.5 °-121.0 °E), and the detailed information on the sites is shown in Table 1. The SMC and soil temperature were continuously measured via the Em50 data collection system with EC-5TM probes (Decagon Devices, Inc., Washington, USA) from October 2013 to September 2019. Considering the penetrability of the C band and L band in complex land surfaces over the Genhe watershed, the average SMC and soil temperature observations from top 3-cm and 5-cm layers were selected to be used in this work. Soil surface roughness was measured by a pin profiler at each site. The surface roughness measurements of the root mean square height and correlation length in the study area were approximately 0.8~1.5 cm and 5~15 cm,
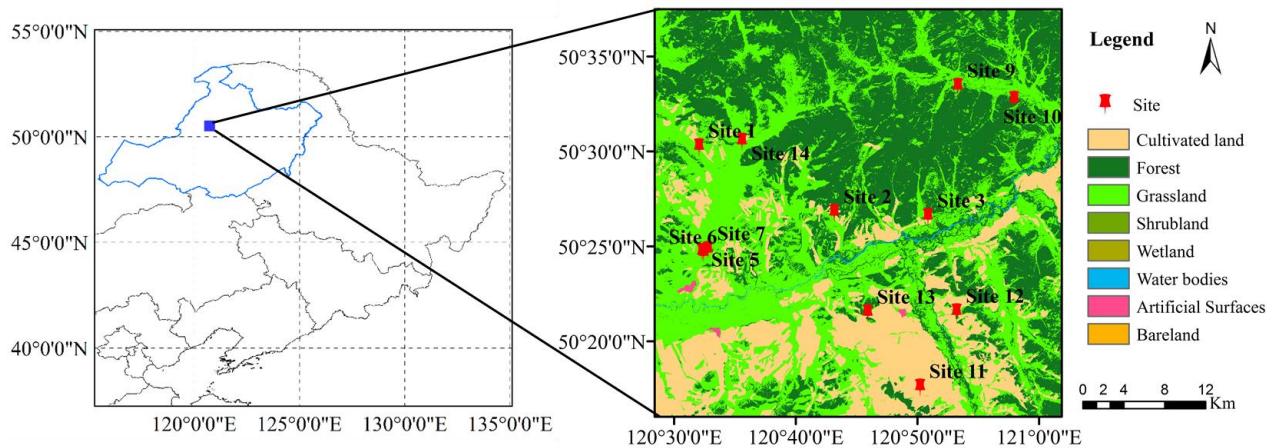
respectively. Vegetation height was derived from in situ measurements at complicate observations and multi-parameter land information constructions on allied telemetry experiment (COMPLICATE) [40] and Genhe watershed observation network [39]. Soil texture was measured in the laboratory with soil samples by the cutting ring method in the field. The topsoil texture of this area is mainly composed of silt (50%~54%), sand (6%~9%), and clay (39% ~ 44%).

TABLE 1. INFORMATION ON THE SITES IN THE STUDY AREA

Site name	Lon. (deg.)	Lat. (deg.)	Alt. (m)	Land cover	Time(Day/ Month/Year)
Site 1	120.522	50.505	705	Grass	07/10/2013-
Site 2	120.711	50.451	699	Larix gmelinii	10/10/2013-
Site 3	120.840	50.450	628	Shrub, Birches	06/10/2013-
Site 5	120.531	50.413	628	Grass, Shrub	07/10/2013-
Site 6	120.533	50.412	673	Grass	07/10/2013- 09/10/2015
Site 7	120.539	50.415	792	Grass	07/10/2013- 19/09/2015
Site 9	120.876	50.565	705	Birch forest	21/04/2015-
Site 10	120.954	50.555	728	Larix gmelinii	21/04/2015- 02/10/2015
Site 11	120.836	50.300	724	Shrub, Birches	10/10/2015-
Site 12	120.883	50.367	651	Shrub	10/10/2015-
Site 13	120.761	50.364	754	Birch forest	10/10/2015- 10/05/2017
Site 14	120.581	50.511	731	Birch forest	09/10/2015-

Fig. 1. Land cover map in the Genhe watershed (from GlobeLand30, http://www.globallandcover.com/)

B. SAR data

The local overpass time and temporal resolution of the Sentinel-1 and ALOS-2 SAR sensors are different. To better compare the retrieval results of the Sentinel-1 and ALOS-2 SAR sensors, data with similar overpass times of the two satellites are screened out within the period from 2015 to 2016 (Table 2). Cui et al [3] have shown that the soil surface in the Genhe watershed is frozen at the beginning of November and thawed at the beginning of April. The state of the SMC is complicated under frozen conditions, due to low dielectric constant values of frozen soils, and thus, this work was

conducted for the unfrozen season only, by removing data that corresponded to frozen dates from the analysis. The satellite passes that correspond to unfrozen conditions are shown in Table 2 with the mark *.

1) Sentinel-1

The Sentinel-1 mission is the European Radar Observatory for the Copernicus joint initiative of the European Commission and the European Space Agency. A C-band (5.405 GHz) SAR is aboard Sentinel-1, and it provides dual polarization capability. Sentinel-1 comprises a constellation of two polar-orbiting satellites, Sentinel-1A (launched on April 3, 2014) and Sentinel-1B (launched on April 25, 2016), which share the same orbital plane, and the repeat cycle at the equator with one

satellite is 12 days [41]. It operates in four exclusive acquisition modes: strip map, interferometric wide swath, extrawide swath, and wave mode with different resolutions (down to 5 m) and coverages (up to 400 km). This study used ground range detected high-resolution standard products with vertical-vertical (VV) and vertical-horizontal (VH) polarization in the interferometric wide swath mode (Level 1, https://scihub.copernicus.eu/dhus/#/home). All Sentinel-1 data were preprocessed using the Sentinel Application Platform (SNAP), as follows: updating orbits, thermal noise removal, radiometric calibration, speckle filtering, terrain correction (using Shuttle Radar Topography Mission digital elevation model at 30 m), and linear to dB conversion. Considering the spatial resolution of other satellite data, the last step is resampled at 30 m. The local incidence angle of Sentinel-1 in Genhe watershed is mainly range between 20° and 60°. The images collected on July 18 and 28 September 28, 2015, July 12 and September 22, 2016 were selected for this research during unfrozen seasons (in Table 2). Information about the satellite data are shown in Table 3.

2) ALOS-2

ALOS-2 is follow-on mission from the "DAICHI", which was developed by Mitsubishi Electric Corporation under contract to Japan Aerospace and Exploration Agency (JAXA). ALOS-2 was launched on May 24, 2014, with a revisit time of 14 days. The state-of-the-art Phased Array type L-band Synthetic Aperture Radar-2 (PALSAR-2) aboard ALOS-2 uses the 1.2 GHz frequency range [42]. ALOS-2 has three main observation modes: spotlight mode (1 to 3 m), strip map mode (3 to 10 m) and scanSAR mode (100 m/60 m) [43]. This study used strip map mode with horizontal-horizontal (HH) and horizontal-vertical (HV) polarizations products (Level 1.5, fine mode, https://satpf.jp/spf/?lang=en). The local incidence angle of ALOS-2 in Genhe watershed is mainly range between 10° and 50°.The dates of the selected ALOS-2 images correspond to the Sentinel-1 ones, and they are July 17 and September 25, 2015, July 15 and September 23, 2016 (in Table 2), details of the data are shown in Table 3. All of the ALOS-2 data were preprocessed using the ENVI and SNAP Toolboxes, as with Sentinel-1.

TABLE 2. SAR DATA WITH SIMILAR OVERPASS TIME (*UNFROZEN CONDITIONS)

Sensor	Date	Sensor	Date
Sentinel-1A	Feb 17, 2015	ALOS-2	Feb. 13, 2015
Sentinel-1A	Jul 18, 2015*	ALOS-2	Jul. 17, 2015*
Sentinel-1A	Sep 28, 2015*	ALOS-2	Sep. 25, 2015*
Sentinel-1A	Dec 9, 2015	ALOS-2	Dec. 4, 2015
Sentinel-1A	Feb 7, 2016	ALOS-2	Feb. 12, 2016
Sentinel-1A	Jul 12, 2016*	ALOS-2	Jul. 15, 2016*
Sentinel-1A	Sep 22, 2016*	ALOS-2	Sep. 23, 2016*
Sentinel-1B	Dec 9, 2016	ALOS-2	Dec. 2, 2016

C. Optical data

The free access to both the Sentinel-2 and Landsat 8 data, the similar wavelengths, and the same geographic coordinate system provide an excellent opportunity to use these two types of data [44]. Therefore, we chose Landsat 8 to calculate NDVI for 2015 instead of Sentinel-2 because Sentinel-2 had no

released observations from the official website in the Genhe watershed area for 2015. Moreover, Sentinel-2 was used to calculate the NDVI for 2016 due to the large number of clouds present in the Landsat 8 images. If Sentinel-2 and Landsat 8 images that are closest to the SAR images are cloudy, then the optical images were acquired two weeks before or after the SAR acquisitions could be used because vegetation is assumed to not change significantly within one or two weeks [23]. Details of the data are shown in Table 3.

1) Sentinel-2

The Copernicus Sentinel-2 mission comprises a constellation of two polar-orbiting satellites placed in the same sun-synchronous orbit, namely, Sentinel-2A (launched on June 23, 2015) and Sentinel-2B (launched on March 7, 2017). Each of the satellites in the Sentinel-2 mission hosted a single payload multispectral instrument (MSI) with 10-day repeat cycle, which covered from the visible and near infrared to the shortwave infrared spectral range [45]. This work used Sentinel-2A MSI data Level 1C (https://scihub.copernicus.eu/dhus/#/home) under cloud-free conditions to calculate the NDVI ((Band8-Band4)/(Band8+Band4), 10 m). It should be noted that all of the Sentinel-2A data were preprocessed with radiometric correction, atmospheric correction and resampling at 30 m using the Sentinel-2 Toolbox. Details of the data are shown in Table 3.

2) Landsat 8

Landsat 8 was developed in collaboration between National Aeronautics and Space Administration (NASA) and the U.S. Geological Survey (USGS), and it was launched on February 11, 2013. The satellite carries the Operational Land Imager (OLI) and the Thermal Infrared Sensor (TIRS), and it has a 16-day repeat cycle [46]. This work used Landsat 8 OLI/TIRS C1 Level 2 data (https://earthexplorer.usgs.gov/) under cloud-free conditions to calculate NDVI ((Band5-Band4)/(Band5+Band4), 30 m); details of the data are shown in Table 3.

TABLE 3. DATASETS INFORMATION (SR: SPATIAL RESOLUTION; RES: RESAMPLING RESOLUTION)

Datasets	Acquisition date	Parameter	SR (m)	RES (m)
Sentinel-1	Jul 18, 2015 Sep 28, 2015 Jul 12, 2016 Sep 22, 2016	backscattering coefficient (VV, VH)	10	30
ALOS-2	Jul 17, 2015 Sep 25, 2015 Jul 15, 2016 Sep 23, 2016	backscattering coefficient (HH, HV)	10	30
Landsat 8	Jul 5, 2015 Sep 7, 2015	band5, band4	30	30
Sentinel-2	Jul 19, 2016 Sep 30. 2016	band8, band4	10	30
Globe-Land30	2010	classes	30	30

D. Land cover information

The land cover map used in this paper is GlobeLand30-2010 with a 30-m resolution in the baseline year of 2010, and it was produced by the National Geomatics Center of China (http://www.globallandcover.com/home_en.html?type=data). The GlobeLand30 classification system includes 10 land cover

types, and the images utilized for classification are multispectral images with 30 m resolution, including the Landsat TM5 and ETM+, China Environmental Disaster Alleviation Satellite HJ-1, and other auxiliary data [47].

III. DATA ANALYSIS AND METHODS

A. Data analysis

1) Sensitivity analysis between backscattering coefficients at C and L bands and SMC

Parameters sensitivity analysis will help us to select the appropriate configuration that is more sensitive to SMC. This section analyzes the sensitivity of the SAR signal to the SMC in the VV and VH polarizations from Sentinel-1, and in the HH and HV polarizations from ALOS-2, respectively, as shown in Fig. 2 and Table 4. In this study area, the land cover is mainly characterized by crops, grass, shrubs, and forest. Furthermore, the forestland is mainly composed of artificial forest farms, and the percentage of virgin forest is not very high. The observation sites in the forest are mainly located close to the boundary of the forestland and not in the center. According to the vegetation type and vegetation height measurement of sites in the study area, the observation sites were subdivided into two categories of vegetation: low vegetation (crop, grass and shrub, height approximately ≤ 2 m), and high vegetation (forest, height approximately > 2 m) to better evaluate the sensitivity of the backscattering coefficients in SMC. It should be noted that 2 m is an empirical value applicable to the Genhe study area.
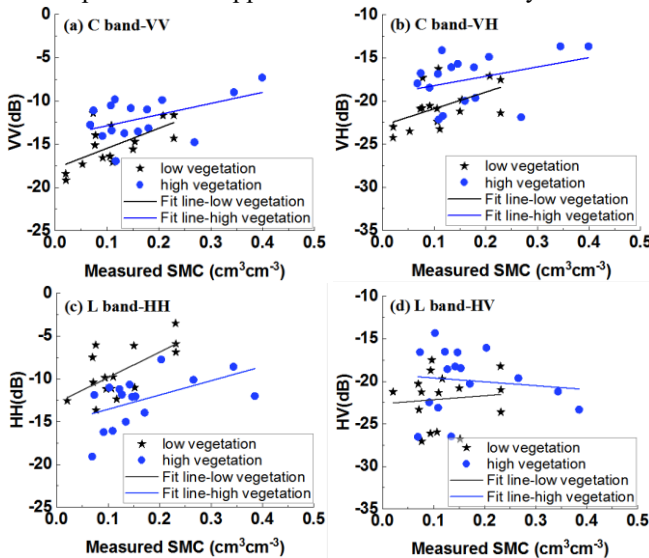

Fig. 2. SAR backscattering coefficient vs. measured SMC for low (asterisks) and high (points) vegetated soil.

Fig. 2 shows the relationship of the SAR backscattering coefficient at C (top) and L (bottom) bands and the measured SMC for low and high vegetated areas. The backscattering coefficient usually increases with increasing SMC at VV, VH, and HH polarizations (in Fig. 2, a-c). The SAR signal at the HV polarization is less sensitive to SMC in the high vegetation area (in Fig. 2d). The threshold of NDVI is 0.3~0.7 for low vegetation and 0.4~0.85 for high vegetation. As expected, there is a significant decrease in the sensitivity of the radar signals to SMC with the increase in the NDVI. This result is clearly

produced by the strong scattering from the high vegetation and the attenuation of soil signals due to high vegetation [15, 23]. A summary of the linear relationships between the backscattering coefficient and SMC at the C and L bands in all of the available polarizations is shown In Table 4. The highest sensitivity to SMC is shown at the VV and HH polarization (in Fig. 2a and 2c), and correlation coefficient R^2 of logarithm fit are 0.45 and 0.43, respectively, whereas there is a significant decrease in the sensitivity of the VH and HV polarizations to SMC (in Fig. 2b and 2d, Table 4). For both of these two frequencies, cross-polarization (VH and HV) is less sensitive to SMC than co-polarization (VV and HH) due to its high sensitivity to volume scattering, which is caused by the strong scattering contribution of the vegetation [10, 15, 48]. The HV polarization data at the L-band show much lower sensitivity to SMC than VH polarization data at the C-band, which may be related to longer wavelength SAR is more sensitive to surface roughness than shorter wavelength SAR. The correlation coefficient R^2 between ALOS-2 HV and roughness, Sentinel-1 VH and roughness are 0.594 and 0.159, respectively. It means that ALOS-2 HV is more sensitive to surface roughness than the Sentinel-1 VH in Genhe area. In addition to the influence of frequency on backscattering, the correlation coefficient (R^2) values between ALOS-2 HH and local incidence angle (18°~38°) and Sentinel-1 VV and local incidence angle (34~48°) are 0.231 and 0.304, respectively. It means that Sentinel-1 VV is more affected by the local incidence angle than the ALOS-2 HH.

TABLE 4. THE RESULT OF BACKSCATTER COEFFICIENT AND SMC FITTING IN DIFFERENT CONDITIONS

Land surface	Relationship	Linear fit	Logarithm fit
Low Vegetation (grass, shrub, crop)	VV vs. SMC	y=23.16*x-17.80, R^2=0.40	y=2.24 ln(x)-9.84, R^2=0.45
	VH vs. SMC	y=19.32*x-22.84, R^2=0.26	y=1.94 ln(x)-16.03, R^2=0.32
High vegetation (forest)	VV vs. SMC	y=12.88*x-14.16, R^2=0.25	y=2.01 ln(x)-8.16, R^2=0.17
	VH vs. SMC	y=10.82*x-19.30, R^2=0.13	-
Low Vegetation (grass, shrub, crop)	HH vs. SMC	y=29.65*x-12.81, R^2=0.42	y=2.78 ln(x)-2.96, R^2=0.43
	HV vs. SMC	-	-
High vegetation (forest)	HH vs. SMC	y=16.66*x-15.22, R^2=0.27	y=3.58 ln(x)-5.58, R^2=0.36
	HV vs. SMC	-	-

(x=SMC, y= backscatter coefficient with different polarizations and frequencies, R^2 is the square of the correlation coefficient, "-" means that the fitting result is poor and R^2<0.1; VV and VH: Sentinel-1 polarization mode, HH and HV: ALOS-2 polarization mode)

Compared with the result of the linear fit in Table 4, the logarithmic fitting shows higher determination coefficients for Sentinel-1 and ALOS-2, except for the Sentinel-1 VH and VV radar signal in high vegetated soil. This finding could be due to the influence of the vegetation and surface roughness and to the complex mechanisms between the radar signal and SMC in

vegetated soil, which are not simply linear [1].

2) Spatial pattern of SAR backscattering coefficient characteristics in the study area

Based on the above analysis, co-polarizations (VV, HH) are demonstrated to be more sensitive to SMC than cross-polarizations (VH, HV). To better understand the co-polarization scattering characteristics of Sentinel-1 and ALOS-2, this section presents the spatial distribution of Sentinel-1 SAR backscatter-VV and ALOS-2 SAR backscatter-HH at a 30-m resolution, as shown in Figs. 3 and 4.

Fig. 3 shows the spatial distribution of the SAR backscatter-VV from Sentinel-1, and it is apparent that the backscatter-VV in July (Fig. 3a and 3c) is mostly higher than that in September (Fig. 3b and 3d). This because July is the thickest time of the year for vegetation, and NDVI is approximately at its maximum, with 0.85 in a high vegetation area over Genhe watershed. Moreover, the backscattering coefficient increases due to the increase in the direct scattering from the upper canopy [49]. Vegetation began to wither in September (NDVI < 0.7), and the backscattering coefficient decreased due to the decrease in the canopy attenuation [50]. Corresponding to the land classification map (Fig. 1), the backscatter-VV in the high vegetation area is higher than that in the low vegetation area. Compared with other land cover types, the backscatter of cultivated land is the lowest. This finding could be related to the scattering mechanism of canopy types.

(a) Sentinel-1 VV on July 18, 2015 (b) Sentinel-1 VV on September 28, 2015

(c) Sentinel-1 VV on July 12, 2016 (d) Sentinel-1 VV on September 22, 2016
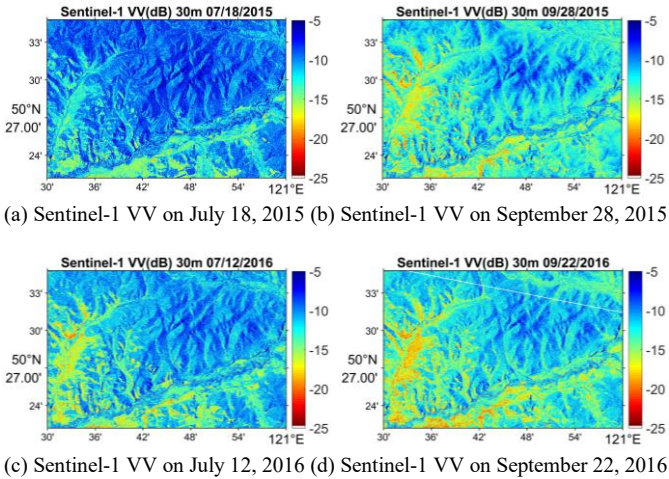
Fig. 3. Spatial distribution of the Sentinel-1 SAR backscattering coefficient for VV on (a) July 18, 2015; (b) September 28, 2015; (c) July 12, 2016; and (d) September 22, 2016

In Fig. 4, the distribution of backscatter-HH from ALOS-2 SAR is consistent with Sentinel-1 backscatter-VV, and the ALOS-2 backscatter-HH in low vegetation areas is lower than that in the high vegetation areas (NDVI approximately 0.85). The backscatter of cultivated land is lower than that of other land cover (grass, forest). The spatial distribution of backscatter-HH in high vegetation areas is similar on July 18 and September 28 2015 (Fig. 4a and 4b), July 12 and September 22 2016 (Fig. 4c and 4d). The ALOS-2 SAR backscattering coefficient seems higher in September than in July, which could be due to the strong penetration capacity of the L band [51], and it is less affected by the scattering of the canopy. Moreover, SMC measurements are wetter in September than in July [3].

(a) ALOS-2 HH on July 17, 2015   (b) ALOS-2 HH on September 25, 2015

(c) ALOS-2 HH on July 15, 2016   (d) ALOS-2 HH on September 23, 2016
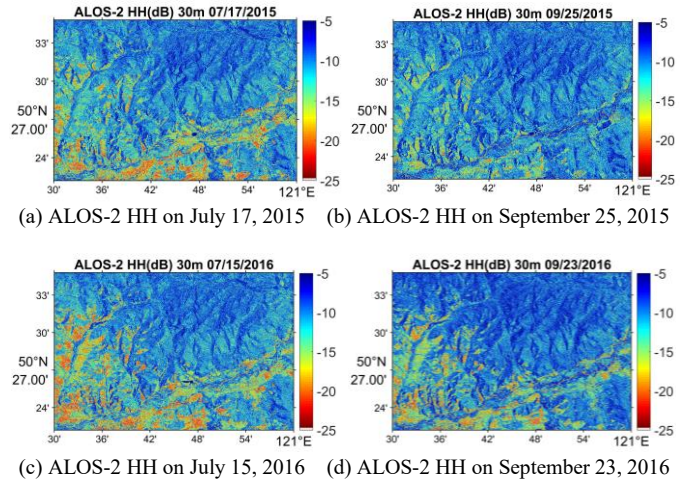
Fig. 4. Spatial distribution of the ALOS-2 SAR backscattering coefficient for HH on (a) July 17, 2015; (b) September 25, 2015; (c) July 15, 2016; and (d) September 23, 2016

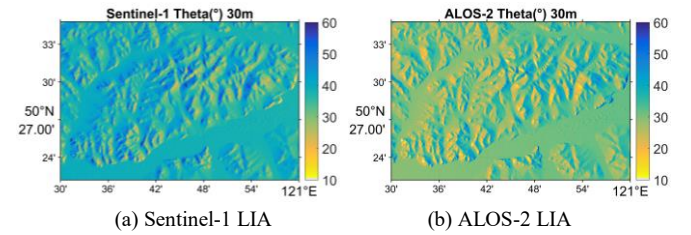(a) Sentinel-1 LIA   (b) ALOS-2 LIA

Fig. 5. Spatial distribution of the SAR local incidence angle (LIA) in Genhe area

The spatial distribution of the Sentinel-1 SAR incidence angle and ALOS-2 SAR incidence angle is shown in Fig. 5. The incidence angles of Sentinel-1 and ALOS-2 are mainly between 20° and 60° (Fig. 5a) and 10° and 50° (Fig. 5b), respectively. Corresponding to the land classification map (Fig. 1), the incidence angle of Sentinel-1 is approximately 10° higher than that of ALOS-2 in grassland, shrubland, cropland and forestland. From the comparison of the spatial distribution of Sentinel-1 backscatter-VV with the ALOS-2 backscatter-HH, the ALOS-2 backscatter is higher than Sentinel-1 backscatter in the high vegetation areas, especially on September 23, 2016 (Fig. 3d and Fig. 4d). This because the ALOS-2 incidence angle is usually lower than the Sentinel-1 incidence angle (Fig. 5a and 5b) and that the backscattering coefficient decreases with increasing incidence angle [52]. Moreover, HH backscatter is higher than VV backscatter at incidence angles of >20°, and HH backscatter is lower than VV backscatter at incidence angles of <20° in vegetated soil [52, 53].

B. Methods

The influence of vegetation, surface roughness, and the complex mechanisms that regulate radar signals and SMC in vegetated soil are not simple to describe [1, 22]. ANN methods provide an alternative to traditional numerical modeling techniques [54], because they can describe the complex relationships between the input and output parameters. During the prediction phase, if a sufficiently robust and representative set of samples were provided during the training phase, the ANN would significantly reduce the computational time [55]

and would be able to estimate and map the SMC from Sentinel-1 and ALOS-2 SAR data with reasonable accuracy. The training set used in the ANN derives from a synthetic database for the C band and L band obtained through the calibrated WCM combined with the AIEM and Oh model. The flowchart of the SMC retrieval method is shown in Fig. 6.
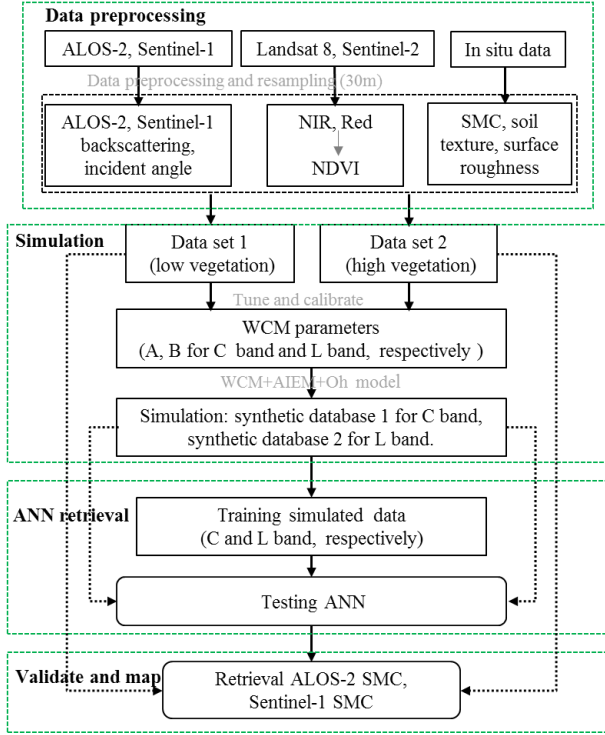

Fig. 6. Flowchart of the SMC retrieval methodology

1) Land surface synthetic database based on electromagnetic model simulations

WCM was developed first by Attema and Ulaby in 1978 [20]. In the WCM, the total backscatter (σ_{pq}^0) is expressed as the incoherent sum of direct backscattering of the vegetation layer (σ_{pq_Veg}) and backscatter from the underlying surface ($\sigma_{pq\_Soil}^0$) which is attenuated by the vegetation layer through the two way attenuation factor (τ^2), and multiple scattering in soil-vegetation is generally neglected. The original model was subsequently modified or extended by various authors [25, 56-58]. In this work, WCM was simplified to [58]:

$$\sigma_{pq}^0 = \sigma_{pq\_Veg}^0 + \tau^2 \cdot \sigma_{pq\_soil}^0 \tag{1}$$

$$\sigma_{pq\_Veg}^0 = A \cdot Veg \cdot \cos\theta(1-\tau^2) \tag{2}$$

$$\tau^2 = \exp(-2 \times B \cdot Veg \cdot Sec\theta) \tag{3}$$

where pq is polarization. θ is the incidence angle. Parameters A and B are parameters that depend on the canopy descriptors and radar configurations. Veg is the vegetation's descriptor (such as vegetation water content (VWC), Leaf Area Index (LAI), and NDVI, etc.). In this work, NDVI was used as vegetation parameter in WCM because it can be easily derived from optical images with resolution 30m.

Some studies have shown that WCM, AIEM and Oh model

have high potentials for soil moisture retrieval [22, 58-60]. Therefore, WCM, AIEM (HH, VV) [18], Oh (VH or HV) [61] was used in this work. In the WCM, the radar backscatter of the bare soil were simulated by the AIEM (HH, VV) and Oh model (VH or HV) at the C band and L band. Parameters A and B are estimated empirically, by fitting the ground observations and models with Nelder–Mead minimization method [62]. To better characterize the backscattering in the presence of different land cover, the vegetation surface is subdivided into low vegetation surfaces (grass, crop and shrub) and high vegetation (forest) surfaces. In Table 5, the fitting and validation of the A and B parameters in the WCM are shown for the C band (VV, VH) and L band (HH, HV) with the different vegetation covers. The validation of the parameters between the calibrated model and the observed data shows that the accuracy of the co-polarization (VV, HH) is better than for the cross-polarization (VH, HV) and the fitting result in the presence of low vegetation is better than in the high vegetation areas. Moreover, some studies have shown that co-polarization (VV, HH) provides higher accuracy on the SMC retrieval than cross-polarization (HV, VH) [22, 23]. Based on these findings, the considered SMC retrieval configuration is limited to VV and HH polarization.

TABLE 5. FITTING AND VALIDATION OF THE A AND B PARAMETERS IN THE WCM FOR EACH POLARIZATION USING SATELLITE DATA AND IN SITU DATA

Band	Land cover	Pol	A	B	R	RMSE (dB)	Bias (dB)
C band	Low vegetation	VV	0.004	0.125	0.97	0.87	0.40
		VH	0.387	0.055	0.89	1.61	0.60
	High vegetation	VV	0.250	0.155	0.94	0.88	0.07
		VH	0.086	0.020	0.69	1.76	0.05
L band	Low vegetation	HH	0.145	0.204	0.96	0.74	0.07
		HV	0.278	0.023	0.72	2.34	-0.17
	High vegetation	HH	0.061	0.065	0.95	1.10	0.37
		HV	0.213	0.024	0.91	2.34	1.80

(Pol: Polarization mode, R is the correlation coefficient, RMSE is the root mean square error, Bias is the mean bias)

With the A and B parameters (Table 5), the land surface synthetic databases are built by the WCM combined with AIEM and the Oh model for the C and L bands, respectively. The input parameters for the C and L bands have the same ranges of values, and the details of input parameters are as follows: (1) SMC, random between 0.02 and 0.42 cm³/cm³, (2) incidence angle, random between 10° and 60°, (3) root mean square height s, random between 0.6 and 6 cm, (4) correlation length l, random between 2 and 20 cm, 0<s/l<0.4, exponential autocorrelation function was used in this work, and (5) NDVI, random between 0 and 0.85.

2) ANN algorithm

The SMC retrieval algorithm is based on the feed-forward multilayer perceptron ANN proposed in [22], which consists of numbers of hidden layers of neurons between the input and the output. The training of the ANN follows the back-propagation learning rule, which can minimize the error between the desired target parameters and the actual output parameters. At the same time, to obtain the optimal ANN architecture with the terms for the neurons and hidden layers, the ANN configuration often starts with a simple combination of hidden layers and neurons, and there is an addition of neurons and hidden layers to increase the ANN configuration. There is repeated training and testing

with error comparisons, until the optimal ANN configuration is found to have a negligible error between the training and testing sets.

According to the above model simulation, the land surface synthetic database was composed of parameters that include the backscattering coefficient, incidence angle, SMC, roughness and vegetation parameters for the C band (database 1) and L band (database 2), respectively. In this work, an optimal ANN architecture with two hidden layers of eight neurons was selected for matching the C band and L band data. In the ANN training, database 1 and database 2 are randomly sampled into two subsets: 50% of the data was selected as the training data, and 50% of the data was used to test the training results. In accordance with the acquisition modes of Sentinel-1, the input parameters of the ANN are the VV backscattering coefficient, incidence angle and NDVI from database 1, and the output parameter is the SMC. In accordance with the acquisition modes of ALOS-2, the input parameters of the ANN are the HH backscattering coefficient, incidence angle and NDVI from database 2, and the output parameter is the SMC.
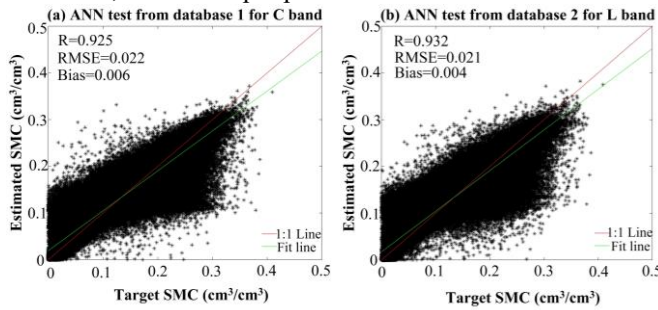

Fig. 7. The training results of the ANN test (a: at the C band, b: at the L band)

The training results of the ANN test for C-band database 1 and L-band database 2 are shown in Fig. 7. In the test, the number of each parameter in database 1 and database 2 is 2,000,000. Here, 50% of the data are randomly selected as training data, and the remaining 50% of the data are used to test the training results. Therefore, database 1 and database 2 are subjected to random sampling in two subsets, each of size 1,000,000. In Fig. 7, the target SMC is derived from C-band database 1 and L-band database 2, and the estimated SMC is retrieved by the ANN. The estimated SMC and target SMC have a significant correlation. The R and RMSE of database 1 are 0.925 and 0.022cm^3/cm^3 (Fig. 7a, for database 1), the R and RMSE of database 2 are 0.932 and 0.021 cm^3/cm^3 (Fig. 7b, for database 2), respectively. The test results show that the ANN's training settings are reliable and they can be used for the subsequent SMC retrieval.

IV.   RESULTS AND DISCUSSION

A. SMC retrieval validation using ground site data

Based on the above ANN algorithm, the SMC is estimated from the Sentinel-1 and ALOS-2 SAR data. The results of the SMC retrievals from the Sentinel-1 and ALOS-2 SAR data are compared with the in situ SMC for low vegetation and high vegetation areas, respectively, as shown in Figs. 8 and 9.

Sentinel-1 and ALOS-2 SMC retrievals had the highest accuracy for the low vegetation covered areas (crop, grass and shrub), with an R of 0.945 and 0.879, and an RMSE of 0.021 and 0.033 cm^3/cm^3 (Fig. 8a and Fig. 9a), respectively. However, with the soil covered with high vegetation (forest), the ALOS-2 SMC retrievals provide, as expected, higher accuracy (with an R of 0.79 and an RMSE of 0.076 cm^3/cm^3) than the Sentinel-1 SMC retrievals (R=0.65 and RMSE=0.14 cm^3/cm^3) in Fig. 8b and Fig. 9b, respectively. This finding is due to the strong attenuation of the SAR signal by high vegetation when the NDVI value was greater than 0.7 [48]. Moreover, the section III showed that the sensitivity of the C-band and L-band SAR signal to SMC for NDVI 0.3~0.7 (low vegetation) is higher than that for an NDVI 0.4~0.85 (high vegetation).
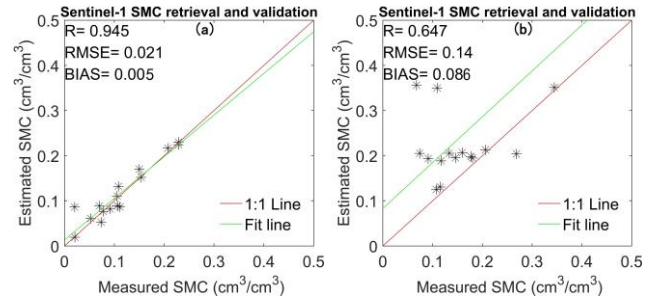

Fig. 8. Validation of the Sentinel-1SMC retrieval (a: low vegetation, b: high vegetation)
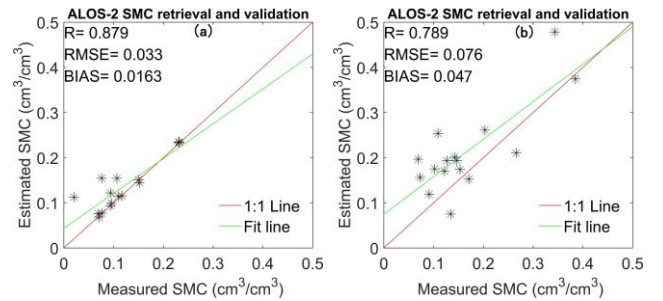

Fig. 9. Validation of the ALOS-2 SMC retrieval (a: low vegetation, b: high vegetation)

By comparing Sentinel-1 and ALOS-2 SMC retrievals, we can note that the accuracy of the Sentinel-1 retrievals is higher than the accuracy of the ALOS-2 retrievals in low vegetation areas. For low vegetation areas, the high sensitivity was obtained from VV polarization of Sentinel-1 (R^2 = 0.45) and HH polarization of ALOS-2 (R^2 = 0.43) in Table 4. The results demonstrated that the potential of Sentinel-1 for SMC estimation was higher than ALOS-2 over low vegetation areas. This finding corresponds to the results of recent studies [48, 63] showing that the SMC estimates from the L-band generally exhibited RMSE values greater than those obtained for the C-band in wheat, grassland and bare soil. For the case without vegetation or with low vegetation cover, the contribution of low vegetation areas to the total scattering is negligible at L-band and C-band. And C-band SAR is more sensitive to soil moisture and less sensitive to surface roughness than L-band SAR [64, 65], which is one of the reason for the accuracy of the Sentinel-1 retrievals is higher than the accuracy of the ALOS-2 retrievals in low vegetation areas. With the soil covered with high vegetation, the RMSE of Sentinel-1 SMC retrievals is 0.064 cm^3/cm^3 higher than ALOS-2 SMC retrievals. This finding is due to the higher frequency (C band), which is less able to penetrate the densely vegetated surfaces with respect to the

longer wavelength L band, and the negligible SMC contribution at the C-band [51].

Overall, VV polarization monitors early canopy growth best, while HH polarization is better during the later stages of canopy development [59, 66]. Moreover, the canopy loss and the volume scattering coefficient increase with the frequency [67], and will decrease the sensitivity of C band to SMC compared with the L band. The accuracy of the ALOS-2 and Sentinel-1 SMC retrievals is higher in low vegetation areas than in high vegetation areas. These results show that both the C band and L band can satisfy the accuracy of the SMC retrieval in low vegetation areas. The L band HH polarization presented better accuracy results than the C band VV polarization in high vegetation soils.

B. Influence of local incidence angle on SMC retrievals

The sensitivity of backscattering coefficient at L-HH and C-VV decreases with increasing incidence angle [68]. The incidence angles of Sentinel-1 and ALOS-2 are mainly 20° ~ 60°and 10°~ 50°, respectively. The radar incidence angle has a large range of variation, and it is difficult to normalize to a fixed angle due to the unavoidable influence of the incidence angle on the retrieval of soil moisture. This is the reason for accounting for the incidence angle as an input parameter in this work, since it is a factor that affects the SMC retrieval. Therefore, the influence of incidence angle on the accuracy of SMC retrievals is discussed in this part.

Based on the in situ measurements and SAR data, the accuracy of SMC retrievals at different incidence angles was calculated, as shown in Table 6. Corresponding to the in situ measurements, the incidence angles of Sentinel-1 are mainly 35° ~ 56°, the incidence angles of ALOS-2 are mainly 20° ~ 37°. Sentinel-1 SMC retrievals have higher RMSE at 35°, 37° and 38°, which are 0.17 cm³/cm³, 0.053 cm³/cm³ and 0.071 cm³/cm³, respectively. ALOS-2 SMC retrievals have higher RMSE at 30°, 32° and 37°, which are 0.087 cm³/cm³, 0.067 cm³/cm³ and 0.058 cm³/cm³, respectively. Coincidentally, these SMC retrievals with higher errors are mainly in forest areas. Moreover, the number of samples is too small at different incidence angles, and it is difficult to find out whether the main influence factor is the local incidence angle or the surface roughness or vegetation.

TABLE 6. ERROR METRICS FOR SENRINEL-1 AND ALOS-2 SMC RETRIEVAL AT DIFFERENT LOCAL INCIDENCE ANGLE (LIA)

SAR	LIA (°)	R	RMSE (cm³/cm³)	Bias (cm³/cm³)	No.
Sentinel-1	35	0.670	0.170	0.126	4
	37	0.840	0.053	0.024	8
	38	0.879	0.071	0.054	8
	43	0.921	0.013	0.003	4
	46	0.964	0.012	0.001	4
	56	0.864	0.016	0.004	4
ALOS-2	20	0.933	0.028	0.012	8
	24	0.750	0.024	0.011	4
	30	0.816	0.087	0.046	8
	31	0.745	0.012	0.010	4
	32	0.822	0.067	0.038	4
	37	0.962	0.058	0.057	4

(No. is the number of samples)

The land surface synthetic database have sufficient samples, therefore, 200 samples were randomly selected at 10°, 20°, 30°, 40°, 50°, 60° in the C-band and L-band simulated database to retrieve and validate SMC and analyze the effect of incidence angle on the accuracy of SMC retrievals. The results of the SMC retrievals from the C-band and L-band simulated database are compared with the simulated SMC at different incidence angle, as shown in Fig. 10 and Table 7.
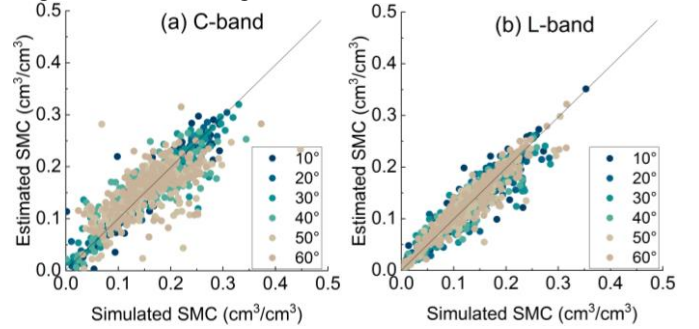

Fig. 10. Validation of SMC estimates from the (a) C-band and (b) L-band simulated database at different local incidence angle

TABLE 7. ERROR METRICS FOR C-BAND AND L-BAND SMC ESTIMATES AT DIFFERENT LOCAL INCIDENCE ANGLE

SAR	LIA (°)	R	RMSE (cm³/cm³)	Bias (cm³/cm³)	No.
C-band	10	0.666	0.047	-0.008	200
	20	0.942	0.022	0.003	200
	30	0.985	0.011	0.009	200
	40	0.932	0.022	0.006	200
	50	0.882	0.034	0.002	200
	60	0.713	0.040	0.002	200
L-band	10	0.765	0.028	0.004	200
	20	0.918	0.020	-0.002	200
	30	0.940	0.019	-0.01	200
	40	0.953	0.017	0.001	200
	50	0.852	0.019	0.001	200
	60	0.783	0.032	0.001	200

From Fig.10 and Table 7, we can see that C- band and L-band SMC retrievals have higher RMSE at low incidence angle (<20°) and high incidence angle (>50°). SAR at low angle of incidence has shorter path length within vegetation volume, and hence, the SAR signal at low incidence angle is able to penetrate up to the soil underneath. Therefore, the low incidence angle SAR backscatter is affected by the soil surface contribution (SMC and roughness) even at vegetated areas [69]. Meanwhile, backscattering coefficient are more sensitive to roughness conditions at L band compared to C band [70]. However, penetration depth could generate some differences and limitations in methodologies, the influence of moisture profile heterogeneities at L-band is less than that C- band because L-band penetration depth is approximately 5 cm for medium moisture levels [71]. Therefore, the accuracy of L-band soil moisture is higher than that of the C-band. Moreover, some studies have indicated that higher incidence angle increases the path length of SAR signal through the vegetation volume, resulting in higher interaction with crop canopy [72]. And SAR signal at high incidence angle is more sensitive to surface roughness and vegetation than at low incidence angle [64, 73]. This is the reason for the accuracy of SMC retrievals is not high at large incidence angle. The influence of incidence angle is considered in the algorithm. Meanwhile, some studies have indicated that the incidence angles from 30° to 50° does not have a significant impact on the sensitivity of HH and VV to the variation of SMC [1], and the errors of the SMC estimates does not significantly depend on the incidence angles (20°~ 45°)

[23]. In this work, the incidence angle (20 ° ~ 50 °) has little effect on the accuracy of SMC retrievals, and the accuracy of C band soil moisture at 30 ° and L band soil moisture at 40 ° is higher than that of other incidence angles. The precondition of the conclusion in the work is that the influence of incidence angle has been considered in the soil moisture retrieval algorithm.

C. The response of SMC retrievals to rainfall

Generally, the occurrence of rainfall will increase the SMC suddenly [74]. To examine the reasonableness of SMC retrievals further, the daily rainfall data from the China Meteorological Data Service Center (0.5 °×0.5 °, http://data.cma.cn/data/cdcdetail/dataCode/SURF_CLI_CHN_ PRE_DAY_GRID_0.5.html) were used to investigate the response of SMC retrieval to rainfall in this part. Corresponding to the local overpass time of the satellite, two weeks of daily rainfall are displayed in Fig. 11, the red circle represents the ALOS-2 mean SMC estimation during its overpass in the study area, and the green circle represents the Sentinel-1 mean SMC estimation during its overpass in the study area.

There are no significant rainfall events, and the cumulative rainfall being less than 10 mm in one week before the Sentinel- and ALOS-2 satellite overpass during the period of July 11-18, 2015 (Fig. 11a) and September 16-23, 2016 (Fig. 11d). Therefore, the influence of rainfall on the SMC retrieval can be ignored during the period July 11-18, 2015 (Fig. 11a) and September 16-23, 2016 (Fig. 11d). During September 21-28, 2015 (Fig. 11b), the cumulative rainfall is 10.3 mm, and there are the slight rainfall events on September 24 and 25, 2015 (4.2

mm, 1.3 mm), which very close to the ALOS-2 overpass. However, there are no rainfall events on September 27 and 28, 2015, which close to the Sentinel-1 overpass. Meanwhile, the ALOS-2 SMC on September 25, 2015 is higher than the Sentinel-1 SMC on September 28, 2018. The results indicate that when the rainfall (<10 mm) arrives one or two days before the ALOS-2 overpass time, the ALOS-2 SMC can capture the influence of rainfall on soil moisture. During July 5-15, 2016 (Fig. 11c), the cumulative rainfall is 19.7 mm, and there are the moderate rainfall (19.2 mm) events on July 8, 2015 four days before the Sentinel-1 overpass, and the slight rainfall (0.5 mm) events on July 11, 2015 one day before the Sentinel-1 overpass. Moreover, the Sentinel-1 SMC July 12, 2015 is higher than ALOS-2 SMC July 15, 2015. The results show that when the rainfall (19.7 mm) arrives four days before the Sentinel-1 overpass time, the Sentinel-1 SMC also can capture the influence of rainfall on soil moisture. Therefore, the Sentinel-1 and ALOS-2 SMC have a good response to rainfall events. There is no rainfall events, the Sentinel-1 SMC is 0.035 cm^3/cm^3 higher than the ALOS-2 SMC on July 17, 2015 in Fig. 11(a), while the ALOS-2 SMC is 0.049 cm^3/cm^3 higher than the S1 SMC on September 23, 2016 in Fig.11 (d). These are because the Sentinel-1 VV-backscattering coefficient is 1.427 dB higher than ALOS-2 HH backscattering coefficient on July 17, 2015 (in Fig. 3a and 4a), and ALOS-2 HH backscattering coefficient is 2.168 dB higher than Sentinel-1 VV-backscattering coefficient on September 23, 2016 (Fig. 3d and 4d).
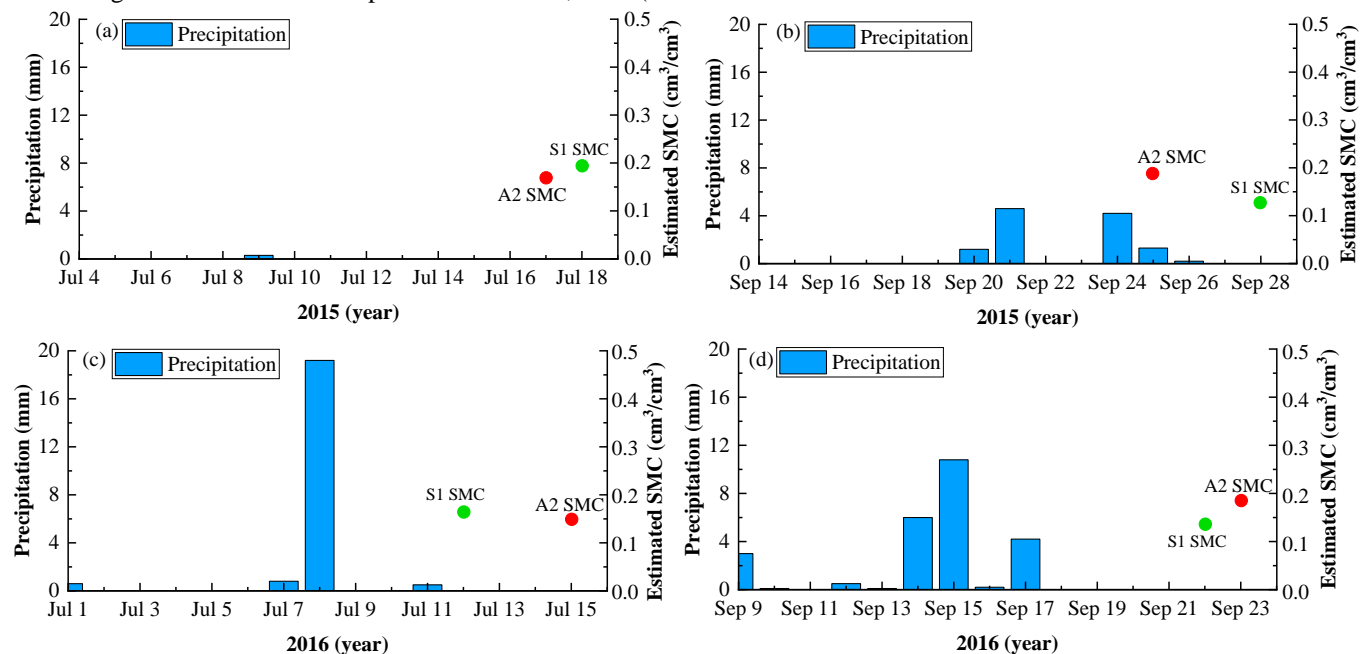

Fig. 11. Daily precipitation in the Genhe watershed area (A2 SMC-red circle: ALOS-2 SMC, S1 SMC-green circle: Sentinel-1 SMC, (a) July 4-18, 2015, (b) September 14-28, 2015, (c) July 1-15, 2016, and (d) September 9-23, 2016)

Overall, when the rainfall is relatively light (<10 mm), the surface evapotranspiration and vegetation interception make it difficult to store water on the land surface [76, 77], and this fact could have an instantaneous effect on the surface SMC, for example, September 2015 (Fig. 11b). However, this aspect has a small effect on the SMC after a few days, and the effects can

be neglected, such as July 2015 and September 2016 (Fig. 11a and 11d). When the rainfall intensity increases, the moderate rain (~19.2 mm) could have a potential impact on the surface SMC due to the infiltration of the rainfall, which could have an effect on the surface SMC in the next few days [75], especially during July 2016 (Fig. 11d). Therefore, in this work, the

cumulative rainfall being less than 10 mm in one week or five days before the satellite pass, the effect of light rainfall (< 10 mm) on SMC can be ignored. If the light rainfall (< 10 mm) arrives one or two days before the satellite pass, it surely has some effects on the soil moisture. And if the moderate rainfall (≥ 10mm) arrives four days before the satellite pass, it has a significant effect on the SMC. Overall, Sentinel-1 and ALOS-2 SMC retrievals have a good response to the rainfall events.

D. SMC mapping

Based on the ANN method, Sentinel-1 SMC maps with a 30 m spatial resolution have been generated on July 18 and September 28, 2015, and on July 12 and September 22, 2016, and they are shown in Fig. 12. ALOS-2 SMC maps with a 30 m spatial resolution obtained on July 17 and September 25, 2015 and on July 15 and September 23, 2016 are shown in Fig. 13. Considering the information on the land cover, the SMC could not be retrieved under the water bodies and the artificial surfaces with the input of land cover information from GlobeLand30-2010.

According to the spatial distribution of the Sentinel-1 SMC and the land classification map (in Fig. 12 and Fig. 1), it can be seen that the Sentinel-1 SMC is mostly higher in July than in September, except for some high vegetation areas. The Sentinel-1 SMC retrievals on July 18, 2015 are higher than the SMC retrievals on July 12, 2016. Corresponding to the land classification map (Fig. 1), the SMC in the high vegetation area is higher than that in the low vegetation area, due to the presence of high vegetation, which can reduce the evaporation and maintain higher levels of water content [78]. ALOS-2 SMC maps on July 17 and September 25, 2015, and on July 15 and September 23, 2016, are shown in Fig. 13. The spatial distribution of the soil wet and dry conditions is consistent with the Sentinel-1 retrievals, and the ALOS-2 SMC is lower in low vegetation areas than in high vegetation areas. The ALOS-2 SMC retrievals in September are higher than the SMC retrievals in July. In addition, the ALOS-2 and Sentinel-1 SMC retrievals show many missing values in the high vegetation area due to the decreasing sensitivity to SMC as the canopy height and NDVI increases (approximately 0.85), except for the water bodies and artificial surfaces.
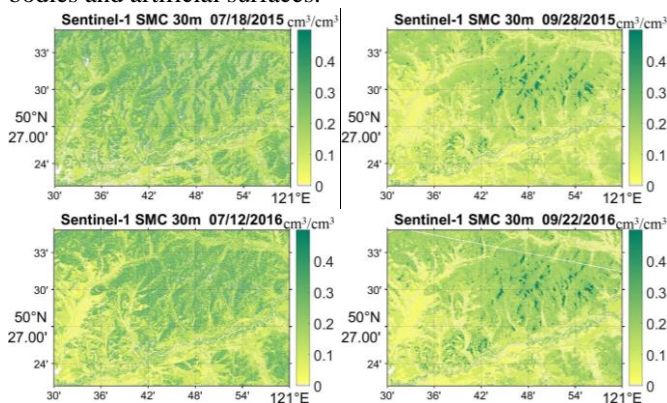

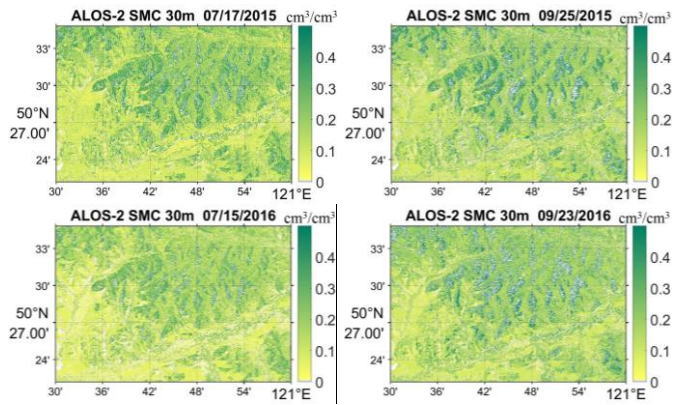Fig. 12. Spatial distribution of Sentinel-1 SMC retrieval

Fig. 13. Spatial distribution of ALOS-2 SMC retrieval

The spatial distribution of SMC retrieval is correlated with the SAR backscattering coefficient, and the backscatter coefficient increases with the SMC (in Fig. 3 and Fig. 12 for Sentinel-1, Fig. 4 and Fig. 13 for ALOS-2). Sentinel-1 backscatter is lower than ALOS-2 backscatter on September 28, 2015 and September 22, 2016. This is the reason for the ALOS-2 SMC retrievals on September 25, 2015, and September 23, 2016, are higher than the SMC retrievals on September 28, 2015, and September 22, 2016. Meanwhile, Sentinel-1 backscatter is higher than ALOS-2 backscatter on July 18, 2015. This is the reason for the Sentinel-1 SMC retrievals on July 18, 2015 are higher than the SMC retrievals on July 18, 2015. This finding corresponds to the backscattering coefficient usually increases with increasing SMC at VV and HH polarizations [63]. Although the SAR images have been processed by speckle filter, the speckle noise still appeared in Sentinel-1 and ALOS-2 soil moisture maps at high vegetation areas. Some studies have shown that upscaling the SAR signal or using an effective speckle filter operator can reduce the speckle noise [14, 79], which is helpful for soil moisture retrieval at high spatial resolution by SAR.

The C-band backscatter SAR signal is less sensitive to SMC under dense and high vegetation covers and high incidence angle (NDVI > 0.7, LIA > 50°), and SAR data are more sensitive to soil roughness at high incidence angles [73]. Consequently, the SMC retrievals become unreliable. On the other hand, the accuracy of ALOS-2 in SMC retrievals is higher than the accuracy provided by Sentinel-1 in the high vegetation area (section IV A). Because L-band observations correspond to a deeper layer of land surface compared to C-band [48, 63]. However, ALOS-2 SMC retrievals have higher RMSE at low incidence angle (LIA < 20°) in the high vegetation area (Refer to Fig. 5 and section IV-B).

E. SMC map validation using the SMAP L2 Radiometer/Radar SMC product

The validation of SMC retrievals is limited by the lack of ground observations. Previous studies have shown that the accuracy of SMAP SMC is higher than AMSR2 and SMOS SMC in the Genhe watershed area [3]. Moreover, the SMAP and Sentinel-1 SMC product (SMAP L2_SM_SP) have a high resolution of 1km/3km, which combines the advantages of L band radiometer measurements and of C band radar measurements [80]. Therefore, in order to understand and analyze the reasonability of the spatial distribution of SMC retrievals at high resolution from SAR, we selected the

currently published SMC product with a high spatial resolution (1 km), namely, SMAP L2 active and passive SMC products (https://nsidc.org/data/SPL2SMAP_S/versions/3) as SMC reference data to intercompare the spatial distribution of the ALOS-2 and Sentinel-1 SMC. The SMAP L2 active and passive SMC algorithm is based on disaggregated brightness temperatures and ancillary data using a single-channel algorithm to retrieve the SMC. The disaggregated brightness temperature of the SMAP L-band radiometer is obtained by using the finer spatial resolution of the Sentinel C-band SAR data and parameters derived from a relationship between the brightness temperature and the SAR data [80].

The SMAP L2 radiometer/radar SMC product was validated by the in situ measurements before use in this work. The results show that SMAP can represent surface soil moisture to some extent. The R and bias between SMAP SMC and in situ measurements are 0.649 and 0.035 cm^3/cm^3, respectively The RMSE of SMAP L2 SMC product is 0.075cm^3/cm^3 in the Genhe area. It should be noted that the validation of SMAP L2 SMC retrievals is limited by the lack of ground observations. This part mainly analyzes the reliability of the spatial distribution of soil moisture. To facilitate intercomparison, the spatial resolutions of the ALOS-2 and Sentinel-1 SMC are aggregated from 30 m to 1 km. The overpass time of Sentinel-1 is closer to SMAP L2 than that of ALOS-2. Therefore, the comparison between ALOS-2 and SMAP can only be used as a reference analysis due to the difference in the overpass times.

The results of the ALOS-2 and Sentinel-1 SMC estimation versus the SMAP SMC are shown in Fig. 14 and Table 8. As shown in Table 8, the correlation between Sentinel-1 SMC, ALOS-2 SMC and SMAP is higher in September (Fig. 14c, 14d, 14 g and 14 h) than in July (Fig. 14a, 14b, 14e, and 14f). This finding is due to the vegetation growing (0.4 < NDVI < 0.87) in July and the vegetation drying (0.3 < NDVI < 0.72) in September, and consequently, the effect of vegetation on the SMC retrieval is reduced in September. The RMSE of Sentinel-1 is lower than that of ALOS-2 (Table 8). The main reason is that the overpass time of Sentinel-1 is closer to SMAP L2 than that of ALOS-2. In fact, the overpass time difference will affect the validation results, especially in 1-3 days. In addition, the time series variation of in situ SMC shows that SMC observations in September are wetter than in July from 2015 to 2016 [3]. This is because rainfall more frequently in September than July (Fig 11). In July, there is less precipitation and soil moisture is relatively dry. Therefore, the RMSE is also generally lower in July than September in particularly for ALOS-2. Sentinel-1 and ALOS have a lot of saturated soil moisture at high vegetation areas, which is different with SMAP SMC (in Fig 15). SMAP L2 SMC combines the C band radar measurements with high-resolution spatial details and the advantages of L band radiometer measurements that are sensitive to surface SMC [80]. It is the main difference with ALOS-2 (L band SAR) and Sentinel-1(C band SAR). Besides, vegetation correction methods are different in soil moisture retrieval. NDVI was used for vegetation correction in the ALOS-2, Sentinel-1, and SMAP SMC retrieval algorithm. The main difference is that the vegetation contributions from the foliage and stem components are taken into considered in the SMAP algorithm [81]. In order to distinguish the different

effects of the vegetation correction methods, the vegetation transmissivity at L-band frequencies (SMAP) was calculated by equation (8) in [81] from the vegetation opacity in SMAP L2 SP soil moisture product, and the vegetation transmissivity at C-band and L-band SAR was calculated by equation (3) in this work. The range of vegetation transmissivity at SMAP L-band (0.25~0.92) is wider than that of Sentinel-1 C-band (0.45~0.84) and ALOS-2 L-band (0.52~0.94), which may be the main reason for the range of SMAP SMC is wider than Sentinel-1 and ALOS-2 SMC, and has less saturation value in this work.

TABLE 8. ERROR METRICS FOR SENTINEL-1 AND ALOS-2 SMC RETRIEVAL

Parameter	Date	R	RMSE (cm^3/cm^3)	Bias (cm^3/cm^3)
Sentinel-1 vs. SMAP SMC	Jul. 18, 2015	0.29	0.045	0.013
	Sep. 28, 2015	0.37	0.053	-0.078
	Jul. 12, 2016	0.30	0.064	0.016
	Sep. 22, 2016	0.47	0.049	-0.120
ALOS-2 vs. SMAP SMC	Jul. 17, 2015	0.33	0.061	0.008
	Sep. 25, 2015	0.40	0.078	0.012
	Jul. 15, 2016	0.27	0.062	0.007
	Sep. 23, 2016	0.52	0.080	-0.033

From the spatial distributions of the ALOS-2, Sentinel-1 and SMAP SMC (in Fig. 15), there are some missing data for the SMAP L2 SMC in the studied area (in Fig. 15c) due to the difference in swath width between SMAP and Sentinel-1. ALOS-2, Sentinel-1, and SMAP SMC are usually higher in high vegetation (forest) than in low vegetation (grass, crop and shrub) areas, which corresponds to the land classification map. Perhaps the presence of well-developed vegetation over the soil contributes to keeping more water content due to the reduced surface evaporation [82]. The spatial distribution of SMC shows that the Sentinel-1 SMC is usually lower than that of the SMAP in September (Fig. 15b and 15c), and the ALOS-2 SMC value is closer to the SMAP SMC, except for some forest areas (Fig. 15a and 15c). SMAP and ALOS-2 SMC are higher in September than in July from 2015 to 2016, which is consistent with the time series variation of in situ SMC [3]. The land surface temperature in July is higher than in September [3], and surface evapotranspiration increases with the increase in the surface temperature, which leads to the surface drying. However, Sentinel-1 SMC is lower in September than in July, which indicates that SMAP and ALOS-2 SMC are more consistent with the measured SMC than Sentinel-1, and the correlation between the ALOS-2 SMC retrievals and SMAP is higher than the correlation from Sentinel-1 in September (Fig. 14 c-d and 14 g-h). Due to the high attenuation effect of the dense vegetation cover (NDVI > 0.7), the C band SAR signal becomes insensitive to the surface SMC, whereas the L band SAR signal is still sensitive to the SMC [51].

Overall, the spatial distribution of ALOS-2 SMC is closer to the SMAP SMC than Sentinel-1. SMAP L2 active and passive SMC product combines the advantages of radiometer measurements and radar measurements, showing an accuracy of ~0.075 cm^3/cm^3 in the Genhe area. If users want to use SMC products with coarser spatial resolution (i.e., ≥ 1 km), they can refer to SMAP L2 active and passive SMC products. If users need higher spatial resolution SMC data (i.e., <1 km), L band SAR is the better choice for SMC retrieval in an agro-forestry area.
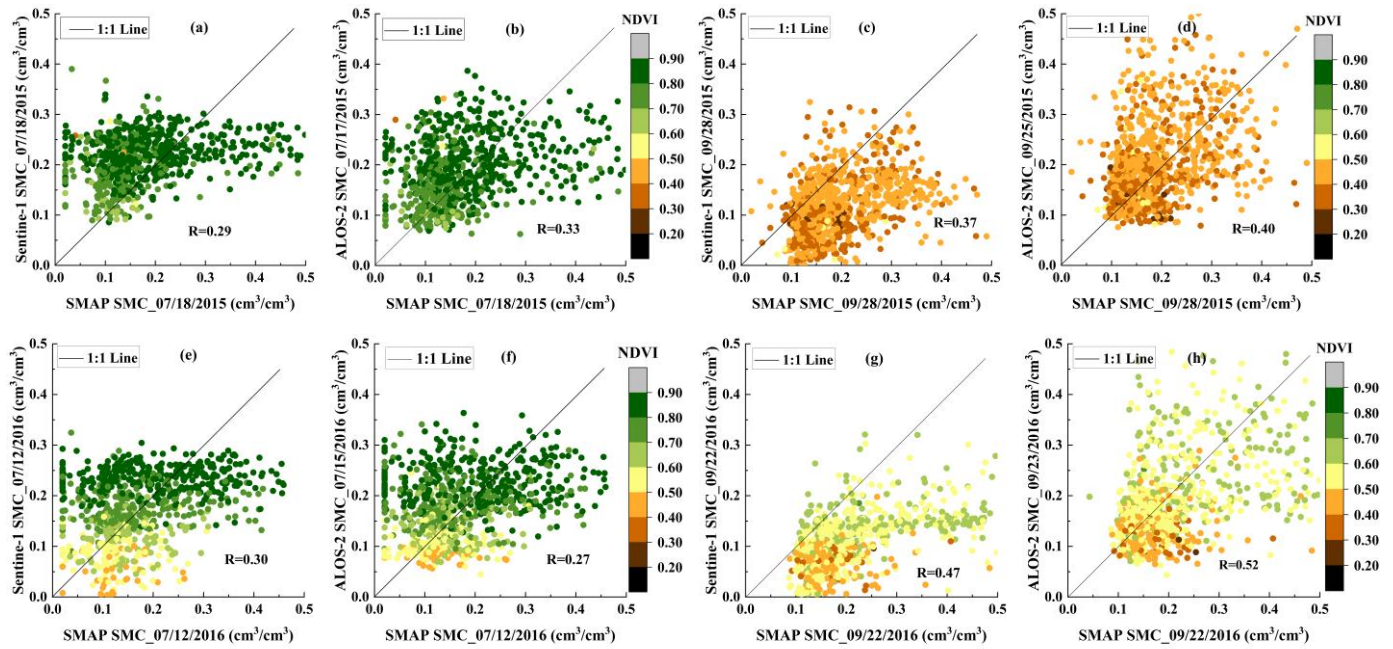
Fig. 14. 1-km resolution aggregated ALOS-2, Sentinel-1 SMC versus SMAP SMC (a, c, e, and g: Sentinel-1 vs. SMAP; b, d, f, and h: ALOS-2 vs. SMAP)

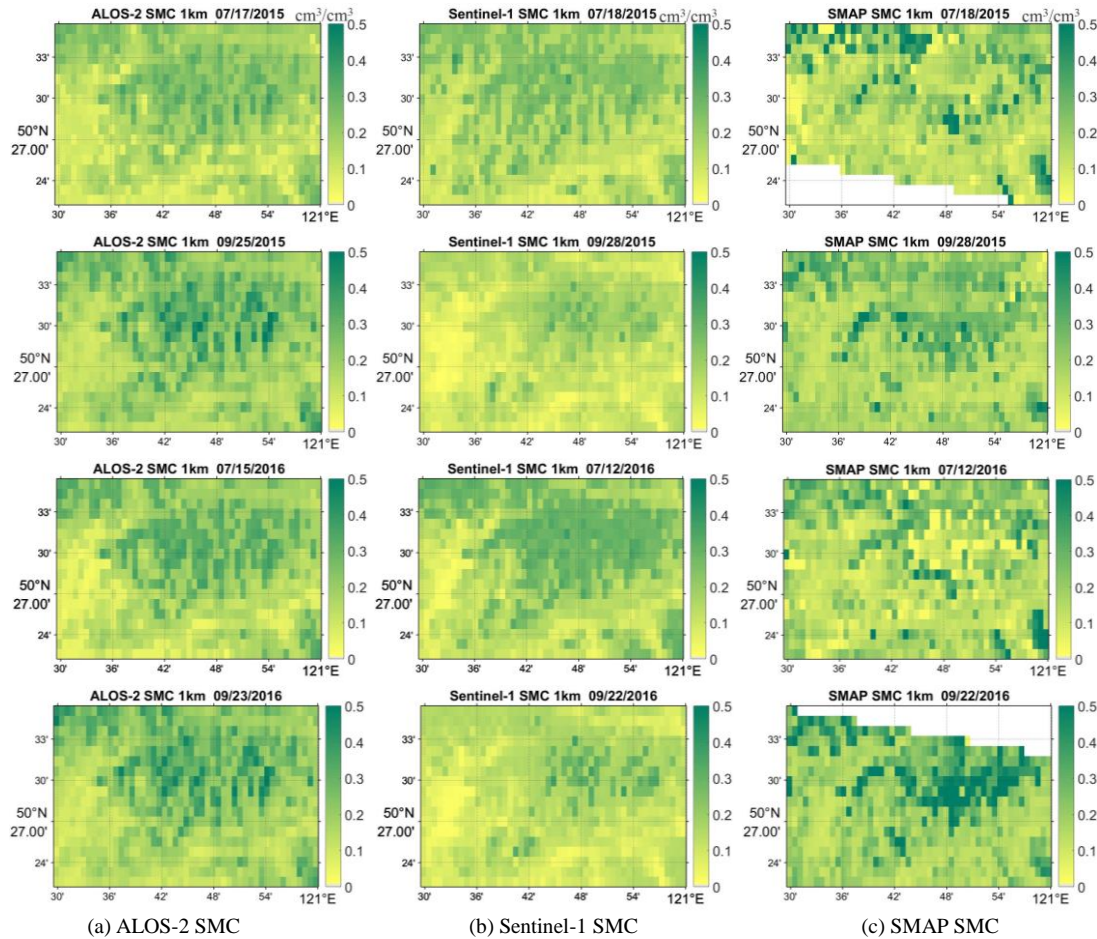(a) ALOS-2 SMC   (b) Sentinel-1 SMC   (c) SMAP SMC

Fig. 15. Spatial distribution of ALOS-2, Sentinel-1 and SMAP SMC with a 1-km resolution ((a) left column: ALOS-2 SMC, (b) middle column: Sentinel-1 SMC, and (c) right column: SMAP SMC)

V. CONCLUSIONS

In this work, the ANN algorithm was used to investigate the potential of Sentinel-1 (C-band) and ALOS-2 (L-band) SAR for SMC retrieval in agro-forestry areas. Based on the parameters analysis, the co-polarization backscattering coefficient (VV or HH), the incidence angle, NDVI and SMC from the simulated databases are used for ANN training and testing. According to

the result of ANN training and testing, the ALOS-2 and Sentinel-1 SMC at 30-m resolution were obtained from the ALOS-2 and Sentinel-1 SAR backscatter, LIA and NDVI, respectively. Subsequently, both ground measured data and SMAP L2 active and passive SMC data were used to intercompare the Sentinel-1 and ALOS-2 SMC, respectively. The results of the comparison between the Sentinel-1, ALOS-2 SMC and measured SMC show that Sentinel-1 and ALOS-2 can provide SMC estimates with high accuracy over low vegetation soils (crop, grass and shrub). The accuracy of the ALOS-2 SMC retrieval over high vegetation soils (forest) is higher than that of Sentinel-1. This finding occurs because of the higher frequency of the C band, which is less able to penetrate the densely vegetation surfaces; thus, the backscatter received by the SAR contains a negligible SMC contribution under these conditions. The results of the intercomparison between the ANN SMC retrievals and the SMAP L2 SMC product show that the correlations between Sentinel-1, ALOS-2 SMC and SMAP SMC when the vegetation is drying in September are higher than when the vegetation is growing in July. The RMSE between Sentinel-1 SMC and SMAP SMC is lower than that of ALOS-2 because the overpass time of SMAP L2 is close to Sentinel-1. The influence of local incidence angle on the SMC retrieval shows that the incidence angle ($20°\sim50°$) has little effect on the accuracy of SMC retrievals, C-band and L-band SMC retrievals have higher RMSE at low incidence angle ($10°$) and high incidence angle ($60°$). The influence of rainfall on the SMC retrieval shows that the Sentinel-1 and ALOS-2 SMC have a good response to the rainfall events.

ALOS-2 L-band SAR appears to have more potential than the Sentinel-1 C-band SAR to estimate SMC in agro-forestry areas. The SMC retrieval from the Sentinel-1 C-band SAR in high vegetation areas is unreliable, with higher errors (0.14 cm^3/cm^3) due to the limited penetration of the C-band and the consequent significant effect of vegetation on the SMC sensitivity, and the large incidence angles also affect the accuracy of SMC retrievals. However, C-band SAR has high potential for SMC retrieval in crop, grass and shrub land (low vegetation areas). The limitations of ground measured SMC data produce more uncertainty for the validation of the proposed algorithm. The SMAP L2 SMC product has been used as a reference (not a truth value) to intercompare the Sentinel-1 and ALOS-2 SMC estimates, it cannot completely substitute for in situ data, which introduces some errors and affects the comparison results.

ANN has the power to retrieve the complex, dynamic and nonlinear patterns from the data, but it is "black boxes", and the user has no control, except providing the input data. This is the limitation of the ANN algorithm, which leads to the uncertainty of the SMC estimates. Although the soil moisture maps at 30-m resolution were obtained in this work, it still have a few speckles in the soil moisture maps. Therefore, effective removal of speckles in SAR images is also an issue that needs to be considered in the future soil moisture retrieval at meter scale. Meanwhile, semi empirical and electromagnetic vegetation models are used to build a synthetic database, while ignoring the multiple scattering effects between canopy layers, and

NDVI as the vegetation's descriptor in WCM is easily saturated in forest areas, which could produce some negative impacts on the retrieval results. SMC retrieval in dense and high vegetation is always a key but challenging task, and this work represents only a beginning. In future work, we will consider the previously mentioned factors, by collecting more in situ data and SAR images to investigate the potential of the L-band and C-band SAR sensors in estimating the SMC. Moreover, it is advisable to adopt an optimized vegetation correction method to improve the accuracy of the SMC retrievals and obtain high-resolution SMC maps.

REFERENCES

[1] J. Shi, J. Wang, A. Y. Hsu et al., "Estimation of bare surface soil moisture and surface roughness parameter using L-band SAR image data," IEEE Transactions on Geoscience and Remote Sensing, vol. 35, no. 5, pp. 1254-1266, 1997.

[2] J. Peng, C. Albergel, A. Balenzano et al., "A roadmap for high-resolution satellite soil moisture applications – confronting product characteristics with user requirements," Remote Sensing of Environment, vol. 252, 2021.

[3] H. Cui, L. Jiang, J. Du et al., "Evaluation and analysis of AMSR‐2, SMOS, and SMAP soil moisture products in the Genhe area of China," Journal of Geophysical Research: Atmospheres, vol. 122, no. 16, pp. 8650-8666, 2017.

[4] W. W. Verstraeten, F. Veroustraete, C. J. van der Sande et al., "Soil moisture retrieval using thermal inertia, determined with visible and thermal spaceborne data, validated for European forests," Remote Sensing of Environment, vol. 101, no. 3, pp. 299-314, Apr 15, 2006.

[5] R. D. de Roo, D. Yang, F. T. Ulaby et al., "A semi-empirical backscattering model at L-band and C-band for a soybean canopy with soil moisture inversion," IEEE Transactions on Geoscience and Remote Sensing, vol. 39, no. 4, pp. 864-872, 2001.

[6] A. Balenzano, F. Mattia, G. Satalino et al., "Dense Temporal Series of C- and L-band SAR Data for Soil Moisture Retrieval Over Agricultural Crops," IEEE Journal of Selected Topics in Applied Earth Observations and Remote Sensing, vol. 4, no. 2, pp. 439-450, 2011.

[7] A. Tabatabaeenejad, M. Burgin, D. Xueyang et al., "P-Band Radar Retrieval of Subsurface Soil Moisture Profile as a Second-Order Polynomial: First AirMOSS Results," IEEE Transactions on Geoscience and Remote Sensing, vol. 53, no. 2, pp. 645-658, 2015.

[8] G. Macelloni, S. Paloscia, P. Pampaloni et al., "The SIR-C/X-SAR experiment on Montespertoli: Sensitivity to hydrological parameters," International Journal of Remote Sensing, vol. 20, no. 13, pp. 2597-2612, 1999.

[9] M. El Hajj, N. Baghdadi, M. Zribi et al., "Soil moisture retrieval over irrigated grassland using X-band SAR data," Remote Sensing of Environment, vol. 176, pp. 202-218, 2016.

[10] Q. Gao, Z. Mehrez, E. Maria et al., "Synergetic Use of Sentinel-1 and Sentinel-2 Data for Soil Moisture Mapping at 100 m Resolution," Sensors, vol. 17, no. 9, pp. 1966-, 2017.

[11] A. Amazirh, O. Merlin, S. Er-Raki et al., "Retrieving surface soil moisture at high spatio-temporal resolution from a synergy between Sentinel-1 radar and Landsat thermal data: A study case over bare soil," Remote Sensing of Environment, vol. 211, pp. 321-337, 2018.

[12] J. Ezzahar, N. Ouaadi, M. Zribi et al., "Evaluation of Backscattering Models and Support Vector Machine for the Retrieval of Bare Soil Moisture from Sentinel-1 Data," Remote Sensing, vol. 12, no. 1, 2019.

[13] M. Foucras, M. Zribi, C. Albergel et al., "Estimating 500-m Resolution Soil Moisture Using Sentinel-1 and Optical Data Synergy," Water, vol. 12, no. 3, 2020.

[14] B. Bauer-Marschallinger, V. Freeman, S. Cao et al., "Toward Global Soil Moisture Monitoring With Sentinel-1: Harnessing Assets and Overcoming Obstacles," IEEE Transactions on Geoscience and Remote Sensing, vol. 57, no. 1, pp. 520-539, 2019.

[15] M. Zribi, S. Muddu, S. Bousbih et al., "Analysis of L-Band SAR Data for Soil Moisture Estimations over Agricultural Areas in the Tropics," Remote Sensing, vol. 11, no. 9, 2019.

[16] Y. Izumi, J. Widodo, H. Kausarian et al., "Potential of soil moisture retrieval for tropical peatlands in Indonesia using ALOS-2 L-band full-polarimetric SAR data," International Journal of Remote Sensing, vol. 40, no. 15, pp. 5938-5956, 2019.

[17] A. K. Fung, and K. S. Chen, "An Update on the IEM Surface Backscattering Model," IEEE Geoscience and Remote Sensing Letters, vol. 1, no. 2, pp. 75-77, 2004.

[18] W. Tzong-Dar, and C. Kun-Shan, "A reappraisal of the validity of the IEM model for backscattering from rough surfaces," IEEE Transactions on Geoscience and Remote Sensing, vol. 42, no. 4, pp. 743-753, 2004.

[19] Y. Oh, K. Sarabandi, and F. T. Ulaby, "An empirical model and an inversion technique for radar scattering from bare soil surfaces," IEEE Transactions on Geoscience and Remote Sensing, vol. 30, no. 2, pp. 370-381, 1992.

[20] E. P. W. Attema, and F. T. Ulaby, "Vegetation modeled as a water cloud," Radio Science, vol. 13, no. 2, pp. 357-364, 1978.

[21] F. T. Ulaby, K. Sarabandi, K. Mcdonald et al., "Michigan microwave canopy scattering model," International Journal of Remote Sensing, vol. 11, no. 7, pp. 1223-1253, 1990.

[22] S. Paloscia, S. Pettinato, E. Santi et al., "Soil moisture mapping using Sentinel-1 images: Algorithm and preliminary validation," Remote Sensing of Environment, vol. 134, pp. 234-248, 2013.

[23] M. El Hajj, N. Baghdadi, M. Zribi et al., "Synergic Use of Sentinel-1 and Sentinel-2 Images for Operational Soil Moisture Mapping at High Spatial Resolution over Agricultural Areas," Remote Sensing, vol. 9, no. 12, 2017.

[24] S. Paloscia, P. Pampaloni, S. Pettinato et al., "A Comparison of Algorithms for Retrieving Soil Moisture from ENVISAT/ASAR Images," IEEE Transactions on Geoscience and Remote Sensing, vol. 46, no. 10, pp. 3274-3284, 2008.

[25] M. Zribi, A. Chahbi, M. Shabou et al., "Soil surface moisture estimation over a semi-arid region using ENVISAT ASAR radar data for soil evaporation evaluation," Hydrology and Earth System Sciences, vol. 15, no. 1, pp. 345-358, 2011.

[26] W. Wagner, G. Lemoine, M. Borgeaud et al., "A study of vegetation cover effects on ERS scatterometer data," IEEE Transactions on Geoscience and Remote Sensing, vol. 37, no. 2, pp. 938-948, 1999.

[27] H. R. Mirsoleimani, M. R. Sahebi, N. Baghdadi et al., "Bare Soil Surface Moisture Retrieval from Sentinel-1 SAR Data Based on the Calibrated IEM and Dubois Models Using Neural Networks," Sensors (Basel), vol. 19, no. 14, pp. 1-12, Jul 21, 2019.

[28] S.-B. Kim, L. Tsang, J. T. Johnson et al., "Soil Moisture Retrieval Using Time-Series Radar Observations Over Bare Surfaces," IEEE Transactions on Geoscience and Remote Sensing, vol. 50, no. 5, pp. 1853-1863, 2012.

[29] W. Wagner, and K. Scipal, "Large-scale soil moisture mapping in western Africa using the ERS scatterometer," IEEE Transactions on Geoscience and Remote Sensing, vol. 38, no. 4, pp. 1777-1782, 2000.

[30] M. Zribi, and M. Dechambre, "A new empirical model to retrieve soil moisture and roughness from C-band radar data," Remote Sensing of Environment, vol. 84, no. 1, pp. 42-52, 2003.

[31] F. Mattia, G. Satalino, L. Dente et al., "Using a priori information to improve soil moisture retrieval from ENVISAT ASAR AP data in semiarid regions," IEEE Transactions on Geoscience and Remote Sensing, vol. 44, no. 4, pp. 900-912, 2006.

[32] Y. Zeng, J. Li, Q. Liu et al., "A Radiative Transfer Model for Heterogeneous Agro-Forestry Scenarios," IEEE Transactions on Geoscience and Remote Sensing, vol. 54, no. 8, pp. 4613-4628, 2016.

[33] E. Santi, S. Paloscia, S. Pettinato et al., "Comparison between SAR Soil Moisture Estimates and Hydrological Model Simulations over the Scrivia Test Site," Remote Sensing, vol. 5, no. 10, pp. 4961-4976, 2013.

[34] A. Hachani, M. Ouessar, S. Paloscia et al., "Soil moisture retrieval from Sentinel-1 acquisitions in an arid environment in Tunisia: application of Artificial Neural Networks techniques," International Journal of Remote Sensing, vol. 40, no. 24, pp. 9159-9180, 2019.

[35] K. Jia, S. Liang, S. Liu et al., "Global Land Surface Fractional Vegetation Cover Estimation Using General Regression Neural Networks From MODIS Surface Reflectance," IEEE Transactions on Geoscience and Remote Sensing, vol. 53, no. 9, pp. 4787-4796, 2015.

[36] Z. Xiao, S. Liang, J. Wang et al., "Use of General Regression Neural Networks for Generating the GLASS Leaf Area Index Product From Time-Series MODIS Surface Reflectance," IEEE Transactions on Geoscience and Remote Sensing, vol. 52, no. 1, pp. 209-223, 2014.

[37] E. Santi, M. Dabboor, S. Pettinato et al., "Combining Machine Learning and Compact Polarimetry for Estimating Soil Moisture from C-Band SAR Data," Remote Sensing, vol. 11, no. 20, 2019.

[38] M. Zribi, N. Baghdadi, S. Bousbih et al., "Surface Moisture and Irrigation Mapping at Agricultural Field Scale Using the Synergy Sentinel-1/Sentinel-2 Data," Int. Arch. Photogramm. Remote Sens. Spatial Inf. Sci., vol. XLII-3/W6, pp. 357-361, 2019.

[39] L. Jiang, J. Wang, H. Cui et al., "In situ soil moisture and temperature network in genhe watershed and saihanba area in China," Data in Brief, vol. 31, no. 105693, pp. 1-9, 2020.

[40] X. Tian, Z. Li, E. Chen et al., "The Complicate Observations and Multi-Parameter Land Information Constructions on Allied Telemetry Experiment (COMPLICATE)," PLoS One, vol. 10, no. 9, pp. e0137545, 2015.

[41] R. Torres, P. Snoeij, D. Geudtner et al., "GMES Sentinel-1 mission," Remote Sensing of Environment, vol. 120, pp. 9-24, 2012.

[42] Y. Kankaku, S. Suzuki, and Y. Osawa, "ALOS-2 mission and development status," IEEE International Geoscience and Remote Sensing Symposium, pp. 2396-2399, 2013.

[43] S. Suzuki, Y. Kankaku, and Y. Osawa, "Development status of PALSAR-2 onboard ALOS-2," The International Society for Optical Engineering, vol. 8176, no. 81760Q, pp. 1-8, 2011.

[44] Q. Wang, G. A. Blackburn, A. O. Onojeghuo et al., "Fusion of Landsat 8 OLI and Sentinel-2 MSI Data," IEEE Transactions on Geoscience and Remote Sensing, vol. 55, no. 7, pp. 3885-3899, 2017.

[45] M. Drusch, U. Del Bello, S. Carlier et al., "Sentinel-2: ESA's Optical High-Resolution Mission for GMES Operational Services," Remote Sensing of Environment, vol. 120, no. none, pp. 25-36, 2012.

[46] T. R. Loveland, and J. R. Irons, "Landsat 8: The plans, the reality, and the legacy," Remote Sensing of Environment, vol. 185, pp. 1-6, 2016.

[47] C. Jun, Y. Ban, and S. Li, "China: Open access to Earth land-cover map," Nature, vol. 514, no. 7523, pp. 434, Oct 23, 2014.

[48] M. El Hajj, N. Baghdadi, and M. Zribi, "Comparative analysis of the accuracy of surface soil moisture estimation from the C- and L-bands," International Journal of Applied Earth Observation and Geoinformation, vol. 82, 2019.

[49] S. C. M. Brown, S. Quegan, K. Morrison et al., "High-resolution measurements of scattering in wheat canopies-implications for crop parameter retrieval," IEEE Transactions on Geoscience and Remote Sensing, vol. 41, no. 7, pp. 1602-1610, 2003.

[50] F. Del Frate, P. Ferrazzoli, L. Guerriero et al., "Wheat Cycle Monitoring Using Radar Data and a Neural Network Trained by a Model," IEEE Transactions on Geoscience and Remote Sensing, vol. 42, no. 1, pp. 35-44, 2004.

[51] M. El Hajj, N. Baghdadi, H. Bazzi et al., "Penetration Analysis of SAR Signals in the C and L Bands for Wheat, Maize, and Grasslands," Remote Sensing, vol. 11, no. 1, 2018.

[52] F. Ulaby, "Radar response to vegetation," IEEE Transactions on Antennas and Propagation, vol. 23, no. 1, pp. 36-45, 1975.

[53] F. T. Ulaby, G. A. Bradley, and M. C. Dobson, "Microwave Backscatter Dependence on Surface Roughness, Soil Moisture, and Soil Texture: Part II-Vegetation-Covered Soil," IEEE Transactions on Geoscience Electronics, vol. 17, no. 2, pp. 33-40, 1979.

[54] D. D. Alexakis, F. K. Mexis, A. K. Vozinaki et al., "Soil Moisture Content Estimation Based on Sentinel-1 and Auxiliary Earth Observation Products. A Hydrological Approach," Sensors (Basel), vol. 17, no. 6, Jun 21, 2017.

[55] E. Santi, S. Paloscia, S. Pettinato et al., "Application of artificial neural networks for the soil moisture retrieval from active and passive microwave spaceborne sensors," International journal of applied earth observation geoinformation, vol. 48, pp. 61-73, 2016.

[56] F. T. Ulaby, C. T. Allen, G. Eger et al., "Relating the microwave

backscattering coefficient to leaf area index," Remote Sensing of Environment, vol. 14, no. 1-3, pp. 113-133, 1984.

[57] R. Bindlish, and A. P. Barros, "Parameterization of vegetation backscatter in radar-based, soil moisture estimation," Remote Sensing of Environment, vol. 76, no. 1, pp. 130-137, 2001.

[58] N. Baghdadi, M. El Hajj, M. Zribi et al., "Calibration of the Water Cloud Model at C-Band for Winter Crop Fields and Grasslands," Remote Sensing, vol. 9, no. 9, 2017.

[59] A. J. Graham, and R. Harris, "Extracting biophysical parameters from remotely sensed radar data: a review of the water cloud model," Progress in Physical Geography: Earth and Environment, vol. 27, no. 2, pp. 217-229, 2016.

[60] J. Zeng, K.-S. Chen, H. Bi et al., "A Comprehensive Analysis of Rough Soil Surface Scattering and Emission Predicted by AIEM With Comparison to Numerical Simulations and Experimental Measurements," IEEE Transactions on Geoscience and Remote Sensing, vol. 55, no. 3, pp. 1696-1708, 2017.

[61] Y. Oh, K. Sarabandi, and F. T. Ulaby, "Semi-empirical model of the ensemble-averaged differential Mueller matrix for microwave backscattering from bare soil surfaces," IEEE Transactions on Geoscience and Remote Sensing, vol. 40, no. 6, pp. 1348-1355, 2002.

[62] J. A. Nelder, and R. Mead, "A Simplex-Method for Function Minimization," The Computer Journal, vol. 7, no. 4, pp. 308-313, 1965.

[63] A. Sekertekin, A. M. Marangoz, and S. Abdikan, "ALOS-2 and Sentinel-1 SAR data sensitivity analysis to surface soil moisture over bare and vegetated agricultural fields," Computers and Electronics in Agriculture, vol. 171, 2020.

[64] F. T. Ulaby, R. K. Moore, and A. K. Fung, "Microwave Remote Sensing: Active and Passive," Artech House, Dedham, MA, USA, Volume III, 1986.

[65] N. Baghdadi, M. Zribi, C. Loumagne et al., "Analysis of TerraSAR-X data and their sensitivity to soil surface parameters over bare agricultural fields," Remote Sensing of Environment, vol. 112, no. 12, pp. 4370-4379, 2008.

[66] T. Le Toan, H. Laur, E. Mougin et al., "Multitemporal and dual-polarization observations of agricultural vegetation covers by X-band SAR images," IEEE Transactions on Geoscience and Remote Sensing, vol. 27, no. 6, pp. 709-718, 1989.

[67] M. Dobson, and F. Ulaby, "Active Microwave Soil Moisture Research," IEEE Transactions on Geoscience and Remote Sensing, vol. GE-24, no. 1, pp. 23-36, 1986.

[68] Y. Wang, J. L. Day, and F. W. Davis, "Sensitivity of Modeled C- and L-Band Radar Backscatter to Ground Surface Parameters in Loblolly Pine Forest," Remote Sensing of Environment, vol. 66, no. 3, pp. 331-342, 1998.

[69] H. S. Srivastava, P. Patel, Y. Sharma et al., "Large-Area Soil Moisture Estimation Using Multi-Incidence-Angle RADARSAT-1 SAR Data," IEEE Transactions on Geoscience and Remote Sensing, vol. 47, no. 8, pp. 2528-2535, 2009.

[70] F. Mattia, T. Le Toan, J. C. Souyris et al., "The effect of surface roughness on multifrequency polarimetric SAR data," IEEE Transactions on Geoscience and Remote Sensing, vol. 35, no. 4, pp. 954-966, 1997.

[71] M. Zribi, A. Gorrab, N. Baghdadi et al., "Influence of Radar Frequency on the Relationship Between Bare Surface Soil Moisture Vertical Profile and Radar Backscatter," IEEE Geoscience and Remote Sensing Letters, vol. 11, no. 4, pp. 848-852, 2014.

[72] J. F. Paris, "Radar Backscattering Properties of Corn And Soybeans at Frequencies of 1.6, 4.75, And 13.3 GHz," IEEE Transactions on Geoscience and Remote Sensing, vol. GE-21, no. 3, pp. 392-400, 1983.

[73] G. Sun, D. S. Simonett, and A. H. Strahler, "A radar backscatter model for discontinuous coniferous forests," IEEE Transactions on Geoscience and Remote Sensing, vol. 29, no. 4, pp. 639-650, 1991.

[74] M. Miernecki, J.-P. Wigneron, E. Lopez-Baeza et al., "Comparison of SMOS and SMAP soil moisture retrieval approaches using tower-based radiometer data over a vineyard field," Remote Sensing of Environment, vol. 154, pp. 89-101, 2014.

[75] T. J. Jackson, R. Bindlish, M. H. Cosh et al., "Validation of Soil Moisture and Ocean Salinity (SMOS) Soil Moisture Over Watershed Networks in the U.S," IEEE Transactions on Geoscience and Remote Sensing, vol. 50, no. 5, pp. 1530-1543, 2012.

[76] A. Loew, M. Schwank, and F. Schlenz, "Assimilation of an L-Band Microwave Soil Moisture Proxy to Compensate for Uncertainties in Precipitation Data," IEEE Transactions on Geoscience and Remote Sensing, vol. 47, no. 8, pp. 2606-2616, 2009.

[77] C. Rom án-Cascón, M. Lothon, F. Lohou et al., "Can We Use Satellite-Based Soil-Moisture Products at High Resolution to Investigate Land-Use Differences and Land–Atmosphere Interactions? A Case Study in the Savanna," Remote Sensing, vol. 12, no. 11, 2020.

[78] T. Chen, R. A. M. de Jeu, Y. Y. Liu et al., "Using satellite based soil moisture to quantify the water driven variability in NDVI: A case study over mainland Australia," Remote Sensing of Environment, vol. 140, pp. 330-338, 2014.

[79] S. W. Chen, "SAR Image Speckle Filtering With Context Covariance Matrix Formulation and Similarity Test," IEEE Transactions on Image Processing, vol. 29, pp. 6641-6654, 2020.

[80] N. N. Das, D. Entekhabi, R. Scott Dunbar et al., "The SMAP and Copernicus Sentinel 1A/B microwave active-passive high resolution surface soil moisture product," Remote Sensing of Environment, vol. 233, 2019.

[81] O'Neill P, Bindlish R, Chan S, et al., "Soil Moisture Active Passive (SMAP): Algorithm Theoretical Basis Document Level 2 & 3 Soil Moisture (Passive) Data Products," SMAP Science Document, JPL D-66480, Revision F, Jet Propulsion Laboratory, California Institute of Technology, 2020.

[82] M. S. Yee, J. P. Walker, A. Monerris et al., "On the identification of representative in situ soil moisture monitoring stations for the validation of SMAP soil moisture products in Australia," Journal of Hydrology, vol. 537, pp. 367-381, 2016.

Huizhen Cui received the Ph.D. degree in cartography and geographic information system at Faculty of Geographical Science, Beijing Normal University, China in July, 2019. She is currently a Post-Doctor with the College of Life Sciences, Beijing Normal University, Beijing. From 2017 to 2018, she was a Visiting Ph.D. Student with the Institute of Applied Physics, National Research Council (IFAC-CNR), Florence, Italy.

Her research interests include microwave remote sensing of soil moisture and microwave emission and scattering modelling of land surface.

Lingmei Jiang is currently a professor at Faculty of Geographical Science, Beijing Normal University. She received the Ph.D. degree in geography at Beijing Normal University, China in July, 2005.

Her research interests include microwave emission/scattering modelling of land surface, passive microwave remote sensing of snow water equivalent and soil moisture, and surface freeze/thaw state, and remote sensing data assimilated into land surface model. She has authored/co-authored over 150 scientific publications, and has been awarded Shi Yafeng Prize for Young Scientists in Cryosphere and Environment in 2018.

Simonetta Paloscia has been with the National Research Council (C.N.R.), since 1984. Since 2004, she has been scientific responsible of the Microwave Remote Sensing Group, IFAC-CNR (Institute of Applied Physics), and the research line "Microwave Remote Sensing of natural surfaces", in the EO Project of CNR. In 2010, she was nominated the Head of Research, National Research Council. She had a temporary teaching contract of "Microwave Remote Sensing Applications" for the Professional Master "Geomatics and Natural Resources Evaluation" at the "Istituto Agronomico per l'Oltremare" of the Ministry of Foreign Affairs in Florence from 1994 to 2010. She is the author and co-author of more than 100 works published on international journals and books, of more than 200 papers published on proceedings of international meetings. Her research currently focuses on the study of microwave emission and scattering of soil (bare and snow-covered) and vegetation. She was PI and Co-I of many national and international projects (ASI, EC, ESA, and JAXA). Since 1996, she has been a Principal Investigator in JAXA Science Team of AQUA/AMSR-E and GCOM/AMSR-2 for algorithms development of soil moisture and vegetation biomass retrieval. She is member of the SMAP JPL/NASA Science Team.

She was member of organizing and steering committees of internationalmeetings (Specialist Meeting on Microwave Radiometry and IGARSS). She is member of the permanent Steering Committee of MicroRad Meeting and she was General Co-Chair of the MicroRad 1999 and 2008 and URSI-F 2010 meetings organized in Florence. She is an Associate Editor for the International Journal of Remote Sensing, IEEE JOURNAL OF SELECTED TOPICS IN APPLIED EARTH OBSERVATIONS AND REMOTE SENSING, and European Journal of Remote Sensing. She has been a URSI Fellow since 2020. She was the Vice-Chair and Chair of URSI Commission F from 2011 to 2017.

Emanuele Santi (Member, IEEE) received the M.S. degree in electronic engineering in 1997, from the University of Florence, Florence, Italy, and the Ph.D. degree in earth's remote sensing techniques from the University of Basilicata, Potenza, Italy, in 2005. Since 1998, he has been a Researcher with the Microwave Remote Sensing Group, Institute of Applied Physics of the National Research Council, Rome, Italy. He was and is currently involved in many national and international projects (ASI, EC, ESA, and JAXA), acting as a team leader, WP leader or co-I. He is the author or coauthor of 142 papers, published in ISI journals and books and conference proceedings. His research focuses of the development and validation of models and statistical inversion algorithms for estimating the geophysical parameters of soil, sea, snow, and vegetation from microwave emission and scattering.

Dr. Santi, in 2018, was the recipient of the "IEEE GRSS J-STARS Prize Paper Award" for the best paper published in the IEEE JOURNAL OF SELECTED TOPICS IN APPLIED EARTH OBSERVATIONS AND REMOTE SENSING in 2017. He is a member of the Institute of Electric and Electronic Engineers (IEEE) and the "Centro di Telerilevamento a Microonde (Microwave Remote Sensing Center)."He is also Conference Chair of the SPIE Europe Remote Sensing.

Simone Pettinato (Member, IEEE) was born in Florence, Italy, in 1972. He received the M.S. degree in telecommunications engineering from the University of Florence, Florence, Italy, in 2002 and the Ph.D. degree in "methods and technologies for environmental monitoring" from the University of Basilicata, Potenza, Italy, in 2007.

Since 2003, he has been with the Microwave Remote Sensing Group, CNRIFAC, Florence, Italy, as a Scientist. He participated, as a Co-Investigator, in different national and international scientific projects funded by the European Community, European, and Italian Space agencies (ESA and ASI). Between 2009 and 2012, he was involved in three Antarctic expeditions in the framework of the DOMEX-2, DOMEX-3, and GPS-SIDS projects. He is the author or coauthor of more than 100 papers published on international peer-reviewed journals and conference proceedings. His research focuses on the investigation of the natural surfaces by means of active and passive microwave sensors in order to retrieve information of geophysical parameters related to the hydrological cycle (soil moisture, snow, and vegetation).